Desalination and Water Treatment
www.deswater.com

doi: 10.5004/dwt.2022.28045

247 (2022) 40–63
January

Mechanisms, diagnosis, and monitoring of biofouling in membrane processes: a review

Farzin Saffarimiandoab[a,b], Bahar Yavuzturk Gul[b,c], Reyhan Sengur Tasdemir[b,d], Borte Kose Mutlu[b,c], Selda Erkoc Ilter[e,f], Serkan Unal[e,f], Bahadir Tunaboylu[g], Yusuf Z. Menceloglu[e,f], Vahid Vatanpour[a,b,h], Ismail Koyuncu[a,b,*]

[a]*Department of Environmental Engineering, Istanbul Technical University, Maslak 34469, Istanbul, Turkey, emails: koyuncu@itu.edu.tr (I. Koyuncu), saffari101@gmail.com (F. Saffarimiandoab)*
[b]*National Research Center on Membrane Technologies, Istanbul Technical University, Maslak 34469, Istanbul, Turkey, emails: bygul@itu.edu.tr (B. Yavuzturk Gul), reyhansengur@gmail.com (R. Sengur Tasdemir), kosebo@itu.edu.tr (B. Kose Mutlu)*
[c]*Department of Molecular Biology and Genetics, Istanbul Technical University, Maslak 34469, Istanbul, Turkey*
[d]*Department of Nanoscience and Nanoengineering, Istanbul Technical University, Maslak 34469, Istanbul, Turkey, email: reyhansengur@gmail.com (R. Sengur Tasdemir)*
[e]*Nanotechnology Research and Application Center, Sabanci University, Tuzla 34956, Istanbul, Turkey, emails: erkocs@sabanciuniv.edu (S. Erkoc Ilter), serkanunal@sabanciuniv.edu (S. Unal), yusufm@sabanciuniv.edu (Y.Z. Menceloglu)*
[f]*Integrated Manufacturing Technologies Research and Application Center & Composite Technologies Center of Excellence, Sabanci University, Pendik 34906, Istanbul, Turkey*
[g]*Department of Materials Science and Engineering, Marmara University Göztepe Campus, İstanbul, Turkey, email: bahadir.tunaboylu@marmara.edu.tr (B. Tunaboylu)*
[h]*Department of Applied Chemistry, Faculty of Chemistry, Kharazmi University, Tehran, Iran, email: vahidvatanpour@khu.ac.ir (V. Vatanpour)*

Received 5 March 2020; Accepted 12 December 2021

ABSTRACT

Membrane systems have become one of the major technologies in water and wastewater treatment processes. In recent decades, membrane processes have made rapid progress owing to their advantageous properties over conventional systems. However, biofouling restricts their widespread application through irreversible deterioration of their structure, performance, and longevity. Any effort against biofouling either in the membrane synthesis step or in the process necessitates a well understanding of the underlying mechanisms causing this issue through employing various monitoring and diagnosis techniques. This paper mainly reviews the progress in the research and development of biofouling reduction in membrane processes. It first addresses the underlying biofouling mechanisms. Then, a critical overview of the state-of-the-art approaches in the membrane biofouling diagnosis and monitoring was provided to discuss the advantages and the limitations of the current techniques in the lab and large-scale applications. The last section of the review focuses on the future aspects. This paper could be served as a guide for the new entrants to the field of biofouling, as well as to the established researchers and academicians.

Keywords: Biofouling identification; Biofouling mechanisms; Biofouling monitoring; Membrane biofouling

* Corresponding author.

1. Introduction

Biofouling is one of the major ubiquitous challenges faced by membranes in water and wastewater treatment processes. Biofouling is the product of the microorganisms' adhesion and growth on membranes in the form of biofilm [1]. Irreversible destruction in membrane structure and decline in its performance, permeability, and longevity are the main reasons why biofouling is considered the main challenge for membranes. Biofilm formation is induced by microorganism approach and adhesion on a preconditioned nutrient-rich membrane surface and continues further by growing and excretion of protein and polysaccharides rich sticky extracellular polymeric substances (EPS) [2]. Besides the pretreatment of feed water, biofouling is stopped either by active suppressing one of the involved mechanisms through prior modification of membranes or early-stage cleaning of membranes when the microorganisms' attachment is still reversible. Employing effective biofouling diagnosis, monitoring, and characterization techniques and tools are of high importance for identifying either the involved mechanisms or the proper time for cleaning membranes. These tools that are employed currently in lab-scale or large-scale can be classified into performance monitoring, microscopic, spectroscopic, and molecular analysis techniques.

There are various reviews of membrane fouling in the literature [3–8]. While some of them are focused only on some individual membrane processes like membrane bioreactor or forward osmosis [9,10], some of them had presented mixed information from organic and inorganic foulants that have important differences in their nature [5,11]. In our previous study [12], we critically discussed the membrane modification techniques and approaches against membrane fouling. However, this study opens up the topic by elucidation of the biofouling mechanisms, thereafter investigates all the available invasive/non-invasive and in-line/off-line biofouling identification, monitoring, and characterization techniques.

This review introduces the fundamentals of biofouling and the latest molecular spectroscopic approaches on membrane-biofouling characterization with a focus on state-of-the-art spectroscopic imaging and other techniques. Besides, future direction for membrane biofouling characterization should focus on online monitoring to improve anti-biofouling strategy in membrane technologies. The novelty of this review is to include all membrane processes with a limited fouling approach as biofouling.

2. Membrane biofouling mechanisms

Biofilm is a community of irreversibly attached and colonized bacteria on a substrate that is embedded within a biopolymeric matrix [13]. Bacteria in planktonic state converts into the sessile state in biofilm through stepwise stages. The biofouling is governed by the type of microorganisms, aquatic media, and membrane surface. The biofilm development takes place in five stages of the bacteria approach, conditioning layer formation, reversible/irreversible adhesion, growth, and detachment [14] as illustrated in Fig. 1. Initially, a nutrient-rich preconditioning layer is formed on membranes. This layer which contains humic substances, proteins, polysaccharides, and inorganic compounds provides a suitable substrate for bacterial growth. In addition, it enhances bacteria's adhesion by altering surface chemistry, charge, hydrophobicity [15,16]. Adhesion on the surface is the next step that involves various physicochemical and biological interactions between membrane and bacteria. The hydrodynamic

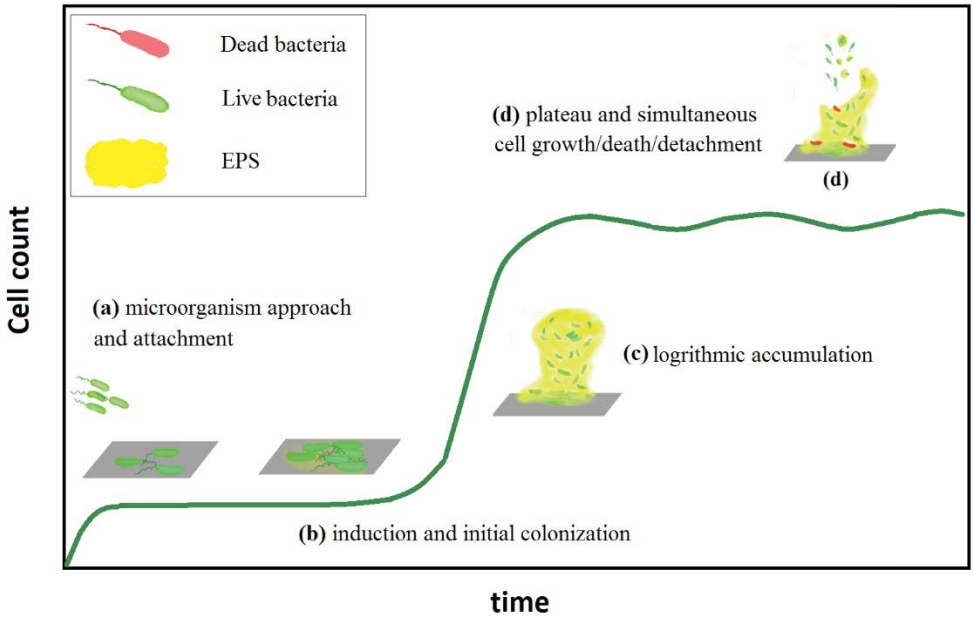

Fig. 1. The biofilm growth step is subdivisions into (a) microorganism approach and attachment (b) induction, (c) logarithmic accumulation, and (d) plateau over time by simultaneous cell growth and death and detachment.

force from the permeation of water through the membrane can enhance microorganisms' approach toward membrane porous structure and surface. However, this acceleration can be counterbalanced by shear forces. The balance between shear force and water permeation can be altered by changing the flux recovery rate of membranes. Hence, optimization of flux recovery rate is considered a crucial factor for fouling mitigation. The physicochemical interactions between bacteria and the membrane surface can be described by the long-range attractive van der Waals' force and short-range repulsive force from the electrical double-layer according to Derjaguin, Verwey, Landau, and Overbeek (DVLO) theory. DVLO theory describes the distance-dependent interaction energy of colloidal particles with 0.5–2 μm in size (analogous to bacteria size) and surface [17]. Adhesion takes place when the total free energy of the interaction between bacteria and the conditioned surface of the membrane is negative. The repulsive force from the electrical double-layer weakens in a medium with higher ionic strength [18]. Rijnaarts et al. [19] compared the significance of steric forces with DVLO interactions at medium with different ionic concentrations. They concluded that adhesion in a medium with low ionic strength is governed mainly by DVLO interaction, while steric interactions become dominant in a medium with higher iconic strength. In addition, their finding showed that attractive van der Waals force differs concerning the hydrophobicity of the surfaces. Hence, it was inferred that a new mechanism should be taken into consideration to explain this. The thermodynamic approach could explain this new interaction based on the hydrophobicity of surfaces.

Besides, cell surface structure and appendages have a determining role in initial attachment on the membrane surface [20–22]. Bacteria appendages and nanowires help the adhesion to be irreversible. Pili and fimbriae are hair-like bacteria appendages. The attached bacteria start to grow by binary fission and to excrete extracellular polymeric substances (EPS) are biopolymers into the surrounding environment during colonization. EPS constitutes 50% to 90% of the total organic matter in biofilm. EPS provides a favorable nutrient-rich medium for bacteria in an oligotrophic environment. It allows the bacteria to live in a stable, dense cell community. The EPS production makes biofilm irreversible by the cohesion of cells and the adhesion of cells on the surface. EPS is a mixture of high molecular weight biopolymers including polysaccharides (40–95%), proteins (1%–60%), nucleic acids (1%–10%), lipids (1%–40%), and other biological macromolecules [23]. Each of these components has different behavior in biofilm. Herzberg et al. [24] demonstrated the preferential adsorption/accumulation of polysaccharides on the *P. aeruginosa*-originated EPS fouling layer. The adsorption efficiencies were 61.2% and 11.6%–12.4% for polysaccharides and proteins, respectively, while the protein concentration was three times higher than polysaccharide concentration in EPS feed concentration. In addition, they observed more adsorbed EPS mass due to more polysaccharide adsorption in the presence of calcium ions. While, in another study, Leroy et al. [25] determined a high amount of protein in EPS from *Pseudoalteromonas sp. D41* marine bacteria.

The presence of ions in the oligotrophic phase can alter the rheology and diffusivity of the EPS by binding ions such as Ca^{2+} and Mg^{2+} [26]. The diffusivity of the EPS layer allows for inter- and intra- gram-negative bacteria information transfer by signaling. The signaling in the bacteria world for communication can be described with a quorum sensing mechanism. It is critical to their gene expression and ability to adjust to changing environmental conditions. The biofilm formation can be given as an example of these abilities and N-acyl-L-homoserine lactone (AHL) is one type of signaling molecule [27]. The diffusion of secreted low-molecular-weight AHLs, bacteria in the EPS layer sense each other and once this signaling passes a specific threshold, a rise in bacterial population growth and a biofilm layer generation occurs on the membrane surface [28]. Bacteria populations in biofilm grow by multiplication in the logarithmic phase and reach a stable level through simultaneous growth and liberation/death in the plateau phase. The occurrence of bacteria liberation may be due to virulence factors and bacteriophages which may spread in the media and then locate in another place. Besides, according to Chen et al. [29], it can also occur due to bacteria's competition for the nutrient. According to their finding, reattachment and domination of a specific bacteria in the biofilm can take place by better adaptation to the environment, nutrient type, and level. The morphology of the biofilm layer can be influenced by the bacterial movement, colonization, or environmental factors. Bacteria can move with the aid of type IV pili over the existing biofilm and new hat-like colonization forms by the new bacteria [30]. The biofilm layer on the membrane is compressed and gets thinner but stronger under hydrodynamic shear forces [31]. Poorasgari et al. [32] showed that the compressibility of the generated cake layer from sludge particles and gel layer from the soluble microbial products (SMP) are reversible and they swell back by releasing pressure in a membrane bioreactor (MBR). They related transmembrane pressure (TMP)-jump at constant flux MBR process to the gel layer compression and consequent rise in permeation resistance over the long term operation. The fluid dynamic and its turbulence have a considerable impact on the initiation of the biofouling as well. Feed spacers in cross-flow operation modes are usually designed to hinder the colonization of microorganisms through the generation of turbulent flow [33,34]. Biofouling across different membrane processes can vary depending on the operational parameters, membrane types, feed solution composition, etc. Chen et al. [35] investigated the fouling mechanism in a submerged anaerobic MBR. The formed cake layer on the membrane was shown to be EPS rich. They showed that osmotic pressure generated by the retained ions was one of the major mechanisms responsible for the membrane fouling problem in MBRs. Herzberg and Elimelech [36] investigated biofouling in RO. They found that bacterial cells in the EPS matrix enhance concentration polarization near the membrane surface, which results in biofilm-enhanced osmotic pressure. The increased salt concentration within the deposited cell layer and the associated increase in osmotic pressure at the membrane surface resulted in a decline in flux.

The biofouling across the different membrane process types that operates under pressure resembles in terms of

mechanisms. However, the biofouling in forward osmosis (FO) and membrane distillations (MD) is considerably diverse due to their different separation mechanisms. In the FO membrane process, the driving force is the osmotic pressure gradient across the membrane and the water permeates from the feed part toward the extremely saline draw solution with a higher osmotic pressure [37]. In the MD process, on the other hand, the driving force is temperature gradient where a highly hydrophobic membrane passes vapors from hot feed solution to the permeated distillate side [38]. The absence of hydraulic pressure gradient in FO causes the biofilm structure to loosely grow similar to the biofilms formed on impermeable surfaces with a thick and mushroom-shaped structure and vertical and horizontal channels [39].

On the other hand, the biofilms on reverse osmosis (RO) or nanofiltration (NF) membranes are severely compact with collapsed channels due to the exposed high-pressure gradient across the membrane. Hence, the decline in water flux is severe in RO due to the high hydraulic resistance from the compressed biofilm. The open structure of FO's biofilms makes nutrients accessible for biofilm cells. Hence the mass ratio of the grown cells to the secreted EPS reportedly is higher in FO than RO [39]. In addition, the attached cells on the FO membrane are subject to high saline stress due to the reverse diffusion of salts from the draw solution toward the feed solution [40]. The biofouling in MD is affected by the hot feed solution, operational mode, and hydrophobic membrane [41]. Even though the high-temperature feed solution in MD suppresses bacterial growth, limited bacterial species can reproduce and contribute to biofouling to some extent. The excreted amphiphilic EPS from the bacteria can reduce the hydrophobicity of membranes. This results in parasitic diffusion of salt ions from the feed stream to the distillate part. According to Bogler and Bar-Zeev's [42] findings in the biofouling analysis of MD against *Anoxybacillus* sp., increasing feed solution temperature from 47°C to 55°C leads to elevated bacterial growth and biofilm generation by which a sharp decline in distillate water flux occurred. In addition, even though a further increase of temperature up to 65°C suppressed bacterial growth, a jump in EPS secretion led to severe impairment in the separation performance by wetting the hydrophobic membrane. It is noteworthy that variation in temperature across the MD system can result in forming biofilms with different compositions and volumes (Fig. 2) [42].

Various researchers had focused on understanding the biofouling mechanisms and anti-biofouling strategies for long years; however, most of them were accrued out in lab-scale and this can result in a gap between the scientific studies and real applications. The pilot-scale studies play an important at this point. For instance; Miura et al. [43] successfully demonstrated that the biofilm development on hollow fiber MF membrane surfaces caused severe irreversible fouling during a long-term operation of pilot-scale MBRs and suggested that a specific phylogenetic group could be responsible for the development of the mature biofilms. So, it can be said that focusing on specific bacterial groups rather than the total microbial community will help the operator to control biofilm formation efficiently. Xu et al. [44] underlined the same suggestion in their pilot-scale NF study.

3. Membrane biofouling diagnosis and monitoring

3.1. Methods based system monitoring: Flux, trans-membrane pressure, and rejection parameters

A decline in permeate flux or TMP-jump in the constant flux process is the sign of the formation of the fouling layer on the membrane [45]. Hence, permeate flux and TMP are employed as biofouling indicators in lab and industrial-scale processes, while they lack the ability of biofouling detection at its early stages. Hence, these techniques are recommended to be applied as complementary techniques along with other precise techniques. Besides, a decline in rejection might be also an indication

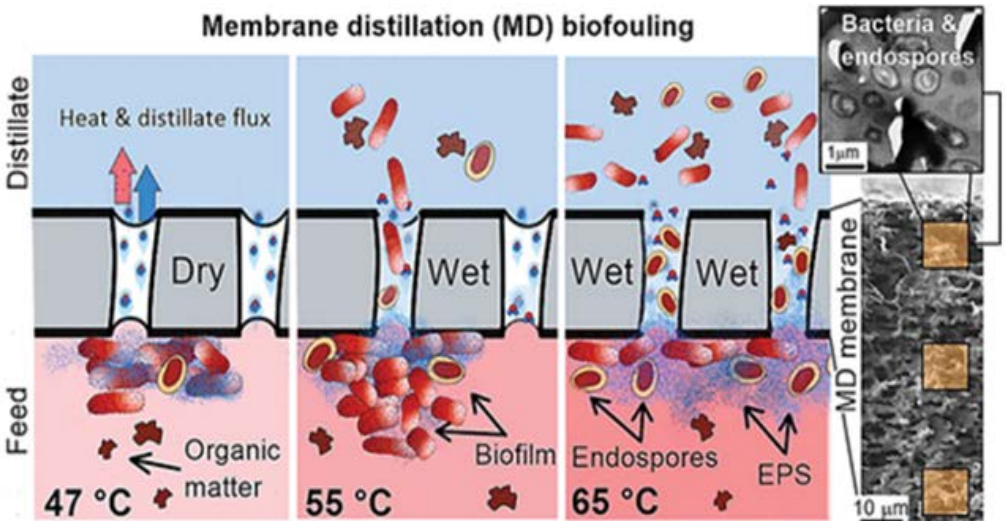

Fig. 2. Illustration of the biofouling mechanism in MD processes [42].

for biofouling if the polymeric membrane material such as cellulose acetate is susceptible to "biodeterioration" by bio-excreted exoenzymes and acids [46,47].

3.2. Microscopic techniques

The visualization in biofilm studies is an indispensable part of the biofouling study. The most prevalent visualization techniques applied for this purpose are light microscopy; epifluorescence microscopy (EFM); confocal laser scanning microscopy (CLSM); multiphoton microscopy (MPM); direct observation (DO) technique; optical coherence tomography (OCT); scanning electron microscopy (SEM); environmental scanning electron microscopy (ESEM); scanning probe microscopy (SPM); near field scanning optical microscopy (NSOM); atomic force microscopy (AFM). The visualization of the biofilm gives useful information about the biofilm structure, in-line visualization specifically provides the biovolume (BV) evolution trend and helps to understand the mechanisms behind this fact. Table 1 presents different microscopic techniques in membrane biofouling studies and lists their capabilities and limitations.

3.2.1. Fluorescent microscopy

Fluorescence microscopy uses specific fluorescent staining for visualization of the target of interest. Various fluorescent microscopic techniques are available. However, in this review, only EFM, CLSM, and MPM techniques that were applied in membrane biofouling were investigated in detail.

In the EFM technique, light illuminates through an objective lens on a sample and gets narrower down by filter to a specific excitation wavelength. The emitted light passes back through the same objective lens and a barrier filters out non-fluorescent lights [66]. Fluorescent staining and EFM have been applied to study the 2D spatial distribution of bacteria and their bioactivity [67–70]. Even though EFM cannot measure biomass depth, cryo-sectioning makes it possible to visualize a cross-section view of accumulated bacteria in biofilm and to measure its thickness. Khan et al. [70] applied EFM to visualize live/dead cells on the biofouled RO and NF membranes. They calculated the thickness and the distribution of accumulated live/dead bacteria across the biofilm by analyzing the cryo-sections of the stained biofilms. It is hard for EFM to distinguish features on the focal point as it suffers from secondary fluorescent generation through the excited volume [48]. The low resolution of EFM is boosted in visualizing thick samples (>2 μm) when high-fluorescence is emitted [54].

On the other hand, CLSM is a non-destructive, fluorescence-based visualization technique that utilizes ultraviolet or visible light to eject blue, red, green, etc. fluorescence [71]. A pinhole is utilized for the elimination of the noisy, out-of-focus emitted lights differentiating CLSM from EFM. CLSM acquires 3D images from every point of the interesting specimen and reconstructs the whole image by an image processing software. CLSM in biological studies is utilized to visualize BV and to elucidate biofouling evolution patterns. Polysaccharide, protein, and bacterial DNA can be labeled by specific fluorescent dyes as shown in Table 2. A dual staining kit differentiates live and dead bacteria based on the integrity of the bacterial cell membrane. Live/dead bacteria are stained collectively at first by the green-fluorescent dye, then a counterstain red-fluorescent dye is applied to stain dead bacteria selectively.

Biofouling development was investigated in a forward osmosis membrane bioreactor (FO-MBR) by Yuan et al. [76] during wastewater treatment. CLSM images of α-D-glucopyranose polysaccharides, β-D-glucopyranose polysaccharides, protein, and total cell were obtained over the 3rd, 8th, and 25th days of operation. The SYTO 63, FITC, Con A, and CW dyes were used to stain total cells, proteins, and α and β-D-glucopyranose polysaccharides, respectively. They concluded that the proteins and polysaccharides contributed equally to biofouling in its initial stage, while protein took the dominant role later. BV showed an increasing and decreasing trend over the process; this reduction at later stages was attributed to the cell and EPS detachment from the biofilm.

The metrics that have been employed to investigate biofouling by CLSM are BV; BV per membrane surface area; mean biomass thickness [77–79]. Moreover, further processing of obtained CLSM images by software such as ImageJ enables us to determine the substratum coverage and components' horizontal and vertical spreading.

In a recent study [58], the antiadhesive and the antibacterial property of zwitterionic polysulfobetain coated RO membranes were proven successfully by live/dead CLSM imaging of membranes at 3rd day and 10th day of biofouling by marine bacteria. Live/dead nucleic acid stains of SYTO9 and propidium iodide were applied. To make images comparable qualitatively, inverted white and black images were also provided. The ability of 3D visualization of thick biofilm, studying the spatial distribution of the biofilm population, and inner layer visualization by cryo-sectioning make this microscopic technique the first choice for biofilm analysis. However, CLSM should not be considered as a quantitative technique as not all the EPS components can be stained. Indeed, gel-like EPS can bind to 80% to >99% of water; hence, determining its exact volume is not possible [80]. In the case of live/dead staining, the aggregates and clumps of cells were referred to as EPS. On the other hand, some critical factors are influencing the functionality of fluorescent dye including bleaching effect, background fluorescent, cross signals of dyes into their channels [49]. Applying CLSM is not enough to compare the bio-characteristics of membrane fouling quantitatively and it is recommended to be practiced along with other complementary techniques such as spectroscopic analysis.

As the final sub-category of fluorescent microscopy, MPM or non-linear optical imaging technique is similar to confocal microscopy and is capable of visualizing specimens three-dimensionally. This technique is designed specifically for deep imaging and for living samples without damaging the living specimen. Due to the phototoxicity effect of laser, two long wavelengths of light are illuminated simultaneously to prevent damage to living cells. By this method, photobleaching, photothermal, and photochemical damages are prevented [51,52]. Also, the penetration depth is increased which makes this method more suitable for

Table 1
Comparison of the capabilities and limitations of the microscopic techniques for membrane biofouling observation

Technique	Capability and advantages	Limitations	References
EFM	- Providing information on the bioactivity of biofilm - 2D visualization	- Low resolution: micrometer range - No sample depth measurement	[48]
CLSM	- No prior sample dehydration - 3D visualization - High resolution	- Requires fluorescent staining - Suffers from fluorescent stain photobleaching - Expensive	[49]
MPM	- In-line monitoring - 3D visualization - Deep sample imaging - Low photobleaching - No damage to living cells	- Need for stopping filtration operation - Expensive	[50–54]
DO	- In-line monitoring - 2D visualization	- Requires a specific membrane cell - Impractical at turbid fluid - Low resolution: 1 μm	[55]
OCT	- Biofilm structure imaging - Non-invasive - In-line monitoring - Label-free - 2D and 3D visualization	- No information on biofilm composition - Low resolution: 1–15 μm - Variation of refractive indices across the *z*-axis	[56]
SEM	- Surface and cross-section imaging - 2D visualization - High resolution: 1 nm	- Requires prior sample dehydration and coating - Sample manipulation - Limited to dry samples	[57,58]
ESEM	- Surface and cross-section imaging - No prior sample dehydration and fixation - Imaging under variable pressure without the need for vacuum - Easy sample preparation - Less time-consuming - 2D visualization - High resolution: 10–20 nm	- Lower resolution than SEM - Sample damage under electron beam	[57,59,60]
NSOM	- Combines the topography and optical property - 3D visualization - High resolution: lateral 20 nm, vertical 2–5 nm	- Sample damage - Shallow sample depth analysis - Time-consuming	[61,62]
AFM	- Imaging surface topography - Obtaining foulant-surface interaction profile - 3D visualization - High resolution	- Sample artifact by AFM tip - Damage from ambient air condition and dehydration	[63–65]

deep visualization than CLSM due to the shallow piercing level of the ultraviolet (UV) and visible short wavelengths [81]. This expensive technique has been used to monitor organic and microbial membrane fouling [53,82].

Hughes et al. [83] investigated the mechanisms of bovine serum albumin (BSA) and ovalbumin fouling on the membrane by comparing MPM results and membrane resistance against the flow. In another study, Hughes et al. [53] applied this technique for imaging the fluorophore-labeled yeast fouling of cellulose ester membrane. The obtained images from the top of the fouling layer with a sub-micron resolution of 45 μm, enabled a clear understanding of the internal structure of the thick cake layer with better quality than non-fluorescent microscopic techniques like direct observation through the membrane (DOTM).

Field et al. [84] applied MPM to investigate the Ultrasil 53 cleaning efficiency of BSA and ovalbumin fouled membrane. A decrease in fluorescent intensity on the membrane after the membrane cleaning revealed the Ultrasil 53's efficiency in removing protein. The optimal cleaning time was found to be 5 min. When longer cleaning times are applied, re-fouling occurs.

Table 2
Fluorescent dyes and their binding targets

Specificity	Binding target	Probes	References
Live and dead	Binds to DNA and RNA	SYTO 9, SYTO 63, Acridine orange, SYBR Green I	[72]
Dead bacteria	Chromosome and nuclear	Propidium iodide red-fluorescent	[73]
Polysaccharide	Binds to α-D-mannosyl and α-D-glucosyl groups	Concanavalin A (ConA), Calcofluor White (CW)	[74]
Proteins	–	Tetramethylrhodamine isothiocyanate (TRITC)-lectin, Hoechst 2495, SYPRO orange, Fluorescein isothiocyanate (FITC)	[75]

3.2.2. Direct observation technique

Direct observation (DO) technique has been practiced for *in-situ*, real-time, non-invasive optical visualization of particle and bacteria deposition and "cake layer" formation in cross-flow membrane separation [85]. Shear flow velocity, microbial short-term and long-term biofilm development, and removal are possible to be investigated by visualization of the cells [86,87]. This technique can be divided into two sub-techniques: DOTM and direct visual observation (DVO).

DOTM was reported for the first time by Li et al. [55] in 1998. A wet Anopore transparent flat sheet membrane is used to enable light passage. A camera-coupled microscope is held onto the permeate side of the membrane to observe the fouling. The effect of yeast and latex particle size and cross-flow velocity on the critical flux and particle deposition was visually investigated. Particle deposition was observed that significantly increased by passing the critical flux level. Wang et al. [88] were inspired by this technique and applied it to the study effect of granular activated carbon size on the membrane fouling in anaerobic fluidized MBR. The transparent membrane has limited applicability for DOTM. Moreover, the camera is held in the permeate side which limits the image acquisition domain to the first layer of fouling formed on the membrane surface.

On the other hand, DVO observation is performed directly from the feed side of the membrane. DVO as DO has become a unique technique for the validation of bacterial deposition model predictions on the membrane. Modeling results confirmed with DO helps find optimal flow conditions. Kang et al. [86] applied the DO technique to observe the stained *S. cerevisiae* bacteria deposition for confirming mathematical model results predicting cell deposition at subcritical flux conditions. The results from the model which was a combination of classical DVLO theory and interfacial hydrodynamic interactions were consistent with DO findings and negated past studies in which particle deposition does not occur under "critical flux". Later on, similar experiments with *S. cerevisiae*, *P. putida*, and *B. subtilis* on NF and RO membranes were carried by Subramani et al. [87] in which higher deposition rates were correlated with higher membrane resistance, salt rejection, concentration polarization, membrane hydrophobicity, higher permeate flux, and membrane surface roughness.

DO was further modified to capture "cake layer" images on the hollow fiber membrane. Le-Clech et al. [89] applied ESEM and CLSM with DO to visualize alginate fouling on the hollow fiber membrane. According to the study, DO was preferred since it can visualize the "cake layer" structure as well as CLSM and does not use expensive fluorescent dye. Different researches were carried out to investigate particle movement near the surface during fouling and cleaning by measuring cake thickness and TMP during bentonite fouling and cleaning on the HF membrane [85,90]. Cake layer evolution was monitored during alginate/bentonite fouling and cleaning on the HF membrane by Ye and Le-Clech [91]. Periodic backwashing with air scouring had a deterministic effect on the cake layer composition and thickness. Recently, Lorenzen et al. [92] investigated the polystyrene particle surface charge on the "cake layer" characteristic during fouling and cleaning on the HF membrane. Cake layer resistance increased by increasing particle surface charge.

3.2.3. Optical coherence tomography

Optical coherence tomography (OCT) is a promising, non-invasive, in-situ, label-free, and real-time technique used to map fouling layer structure as well as flow profiles on the membrane. OCT imaging is based on the comparison of the echo time delay and intensity of backscattered light, a reference reflected light via low coherence interferometry [93]. The echo time delay mechanism of OCT is similar to the ultrasonic reflectometry (which is going to be studied in the next parts) while OCT uses a shorter near-infrared wavelength resulting in higher imaging resolution [94,95] of 1–15 μm [96].

The OCT technique was introduced by Huang et al. [93] in 1991 for medical visualization. Later on, it was applied to visualize biofilm structure determination on membrane three-dimensionally as a method is capable of deep imaging up to several millimeters confirmed in highly scattered tissue. OCT successfully visualized "mushroom" like microbial aggregates at the bottom section of the biofilm layer on the membrane surface. OCT has been applied to analyze the 3D cake layer quantitatively [97], monitor fouling on the MD [98,99], investigate biofilm structure on the membrane [100,101], determine the effects of ionic strength on the *E. coli* adhesion on PVC surface and biofilm roughness [102], to understand the role of the eukaryotic population on biofilm structure and permeate flux [103,104], to visualize and quantify biofouling in feed

spacer channel [105–107] and biofilm structure variation on the membrane after graphene oxide nanoparticle modification [108].

Biofouling formation, structure, and detachment on the membrane surface were investigated by Dreszer et al. [109] using OCT. Mushroom-like structure formation and biofilm detachment were observed over time. Increasing flux led to increased hydraulic resistance by compaction. Fortunato et al. [110] evaluated the suitability of time-laps OCT biofouling monitoring on the submerged MBR. Results revealed a linear relation between biofilm and flux, also longer operation led to the formation of double-layer biofilm. At long-term filtration, a multilayer biofilm structure resulted. This technique does not provide information about the biofilm composition and microbial quantity in EPS, hence applying OCT along with other techniques is necessary [56].

3.2.4. Scanning electron microscopy and environmental scanning electron microscopy

Scanning electron microscopy (SEM) has been utilized as a key visual tool to investigate biofilm since the 1980s [111]. This microscopic technique has been so far applied for the investigation of biofilm structure, the elucidation of the EPS in biofilm [112], the understanding of initial bacteria adhesion on membrane surface [113–115], studying of bacteria development stages on the membrane surface [116], analyzing the antibacterial effect of the surface on the biofilm development over time [117], and the determination of relative cleaning efficiency of biofouled membranes [118]. Sample preparation for SEM starts with fixation, usually by glutaraldehyde as a cross-linker and followed by dehydration as shown in Fig. 3. Finally, the sample is coated by platinum, gold, or gold-platinum conductive matter for inhibition of radiation damage and this coating helps to enhance the contrast for better visualizing.

Saffarimiandoab et al. [58,119] visually analyzed adhesion and biofilm development of unmodified RO membrane and zwitterionic polysulfobetain coated RO membrane by SEM. Biofouling was carried isolated 5 different real marine biofoulant bacteria. Captured SEM images of biofouled membranes at 3rd day and 10th-day biofouling illustrate coatings' antiadhesive and anti-biofouling effect. A considerable number of adhered bacteria and further grown clusters of bacteria are evident in the unmodified membranes. However, a little number of bacteria adhered to the modified membrane evidently, and still bacteria remained individually and separated in a low amount after 10 d of biofouling.

On the other hand, environmental scanning electron microscopy (ESEM) is a modified form of the SEM having operational conditions that allow a sample to be observed in its natural wet state without requiring preparation and conductive coating. An electron beam is positioned in a vacuum, but the specimen chamber is pressurized by gas from 0.1 to 50 Torr [120]. Usually, water vapor is used as a specimen chamber gas. The emitted secondary electrons from the specimen ionize the gas and generate positive charges which ease the artifacts of the sample by attaching. Sample collapsing, artifacts from preparation, consumption of time, and costs of the preparation and coating related to SEM are eliminated by ESEM. However, the probability of electron beam damage still exists as in other electron microscopes [60]. ESEM is advantageous in terms of requiring no need for time-consuming preparations and enabling imaging without dehydration. Nevertheless, SEM has a higher resolution of about 1 nm compared to ESEM which is about 10–20 nm [57]. Moreover, metal staining is reported to enhance the visualization of ESEM by binding them to EPS [121,122]. EPS cracking in SEM treatment may result in images with distinguishable bacteria while preservation of gel-like EPS in ESEM makes it hard to distinguish bacteria [123]. In situ dehydration/hydration is possible in ESEM by changing humidity or specimen temperature [124]. Le-Clech et al. [125] carried ESEM under two wet modes (5°C, 5 Torr, 75% humidity), and dry (or low vacuum) mode

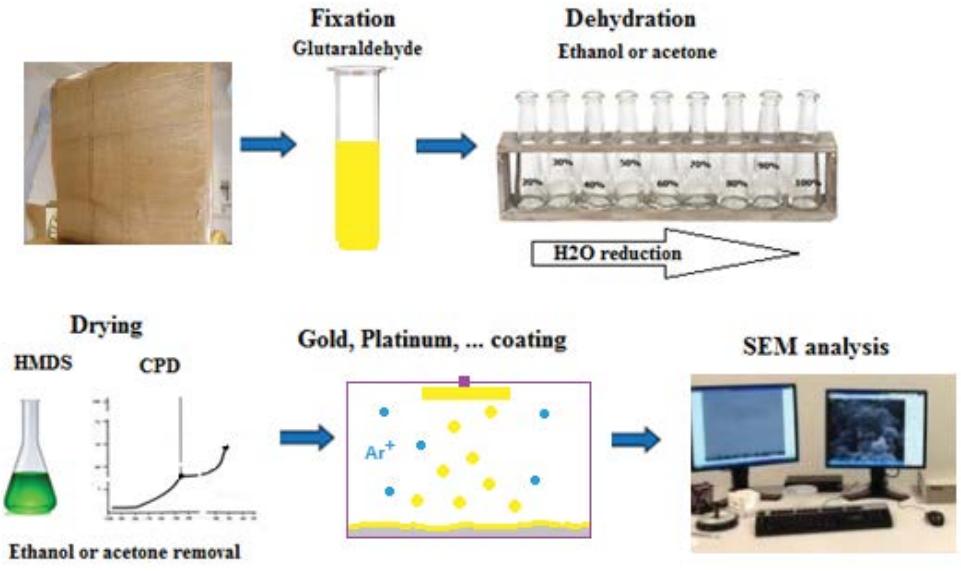

Fig. 3. Sample preparation process in SEM.

(0.5 Torr) to understand the effects of humidity. Under dry mode, relatively clear images were acquired compared to the wet mode.

Fortunato et al. [110] applied ESEM to confirm results from optical coherence tomography images by observing the internal structure of the fouling layer on the flat sheet membrane. The humidity in the chamber intentionally was decreased gradually to form fractures in on the biofilm to make the internal structure visible. The multilayer structure of the biofilm layer was observed on the membrane after long-term filtration confirming the results from OCT.

3.2.5. Scanning probe microscopy

Scanning probe microscopy (SPM) utilizes a tip for probing and imaging the surface by raster scanning [126]. The resolution is directly affected by probe apex sharpness, such as atomic resolution benefiting the tip with one atom at the apex [127,128]. Scanning tunneling microscopy (STM) is the first developed SPM technique [129] which is only applicable for the conductive surfaces [130]. Moreover, the tip penetrates the biofilm until tens of nm up to the substrate, which makes this technique inappropriate for biofilm investigations. AFM and near field scanning optical microscopy (NSOM) were further emerged, which were considered as a breakthrough in the application of the SPM for biological studies.

NSOM is a type of SPM that can be used for concurrent optical and topological analysis of microorganisms and biofilm [131]. The topography is performed by a specialized cantilever featuring a nano-scale aperture. During the scan, a laser is directed through the aperture to excite the sample surface while a photon counter is used to detect the optical response of each excited region [132,133]. The feedback resulted in the image combining the topography of the surfaces with an optical image. The resolution is reported to be 20 nm for lateral and 2–5 nm for vertical dimensions [61]. Ivnitsky et al. [116] assessed the initial biofouling stages by AFM, NSOM, and CLSM. NSOM was used to visualize polysaccharides in the EPS layer by ConA-FITC fluorescent staining. Three-dimensional micrographs were acquired by measuring emitted fluorescent intensity and imaging over the 0, 8, and 16 h filtration. NSOM revealed consistent results with CLSM showing early accumulation of polysaccharides on the membrane and increasing over the filtration time.

Besides, AFM is applied for topographical investigation of the membrane surface up to 0.2 nm lateral resolution and 0.1 nm vertical resolution [63]. The visualization of the sample is performed by measuring the tip and the specimen's surface interaction forces. AFM probing tip can be at contact mode, non-conduct mode, and tapping mode [134]. In contact mode, the cantilever is dragged over the specimen's surface and is deflected by a repulsive force when it passes topographical features. In the non-conduct mode, the cantilever oscillates over the surface which eliminates the sample damage and probe erosion risk. The oscillation amplitude decreases when the tip gets close to the surface. In the tapping mode, the tip oscillates above the cantilever with a much higher amplitude for oscillation. Samples in the wet state and ambient conditions generate a liquid layer. In soft specimens, the tip contacts with the surface softly and it is as close as possible to sense the force without sticking to the surface which minimizes the tip damage [135]. A laser shines down on the cantilever and it reflects onto photodiode which moves up and down by the movement of tip through deflection during scanning. The deflection can occur by the Van der Waals forces, mechanical contact forces, chemical bonding, capillary forces, electrostatic forces, and hydration forces [136]. In contact mode, as the tip gets closer to the surface, the electrostatic repulsive forces become dominant, whereas, in the non-contact mode, the tip is far from the surface which results in the dominance of attractive forces.

AFM primarily has been used to monitor the surface roughness variation over the membrane fouling [137,138]. Moreover, the force-distance curve resulting from cantilever deflection can give valuable insights into membrane and biofilm mechanical property [139]. Tapping mode has been used widely for biological sample imaging [140–142].

Ivnitsky et al. [116] visualized the initial adhesion of bacteria on the polyamide membrane by AFM with a 20 nm probe apex at tapping mode. NSOM, CLSM, and SEM visualization were also performed. Initial bacteria were spotted unanimously. Marka et al. [143] evaluated the effect of feed substrate on the RO membrane biofouling and cleaning. AFM with tapping mode was applied to measure biofilm roughness. 3D and 2D micrographs illustrated with peak and valley structure of biofilm with adhered bacteria. Biofilm increased membrane surface roughness. Biofilm with a more rough structure was more resistant and harder to be cleaned.

Powell et al. [144] carried a comprehensive AFM analysis on the biofouled and virgin RO membrane. Topographical visualization was carried out under air with tapping mode rather than a liquid due to eliminating the risks of impairment in diffusing foulant layers. The images revealed higher roughness and peak-to-valley value for biofouled membranes. To measure mechanical strength, a silica colloid probe with a larger diameter was used on the cantilever to eliminate the risk of damaging the soft surface of the biofilm. Young's modulus of membrane decreased dramatically by biofouling and increasing pH. To remove biofilm easily without damaging the membrane chemically, the pH of cleaning electrolytes should be at a balanced level to render the Young module of membranes and biofilm at their higher level and lower level, respectively.

3.3. Spectroscopic techniques

Spectroscopic techniques are another category in membrane biofouling identification and monitoring. These techniques indicate the chemical composition of the membrane surface or developing a new layer on the surface. Table 3 lists the advantages and disadvantages of various prevalent spectroscopic techniques applied in membrane biofouling identification and monitoring including nuclear magnetic resonance (NMR), Fourier transforms infrared (FTIR), Raman, X-ray photoelectron spectroscopy (XPS), electrochemical impedance spectroscopy (EIS).

Table 3
Comparison of the function and problems of the spectroscopic techniques in the membrane biofouling analysis

Technique	Functions and advantages	Limitations	References
NMR	- In-line visualization of hydrodynamics and water molecules' velocity distribution - Non-invasive and non-destructive	- Time-consuming calculations - Low sensitivity - Complex processing software and devices - High cost - Low signal to noise ratio	[145–149]
FT-IR	- Chemical composition and functional groups determination in biofilm by absorbance - Strain level bacterial identification - Non-invasive - Molecular identification	- Limitation in-depth, 1–2 μm - Interfering of water molecules with IR spectra - Specimen dehydration	[150–154]
Raman	- Gives information on functional groups - Not interfering with water - Enables working with wet samples - Gives narrower spectra with robust band interpretation	- More expensive than IR spectroscopy - Probability of membrane interference	[29,155–158]
XPS	- Gives information on the chemical composition of the biofilm	- Possible interference between membrane and biofilm elements in spectra - Complex - Small sampling depth (typically 5–10 nm)	[69,159]
EIS	- Attributes variation in electrical conductivity of the membrane to the fouling - Lower resolution - Non-destructive	- Existence of complex processing software and devices	[160–162]

3.3.1. Nuclear magnetic resonance

Nuclear magnetic resonance (NMR) studies the physical and chemical properties of molecules and/or atoms of the interesting matter and analyzes the nuclear magnetic response to electromagnetic pulses in the magnetic field between 60–1,000 MHz. Normally ^{1}H and ^{13}C isotopes with an odd number of protons are used for the magnetic behavior of nucleoids due to their intrinsic non-zero spin [163,164]. NMR signal deterioration is characterized by spin-lattice relaxation (T_1) and spin-spin relaxation time (T_2). T_1 and T_2 relaxation times are substance dependent, therefore their variation over the membrane separation process could be an indication for new phase generation such as biofilm. Magnetic resonance imaging (MRI) is an ability of NMR which non-invasively scans an atom for medical imaging [165]. Low sensitivity [146] and high cost [147] are key issues and main drawbacks of this technique for NMR imaging. The function and limitation of NMR along with other spectroscopic techniques are listed in Table 3.

Graf von der Schulenburg et al. [149] monitored biofouling in the RO membrane module for the first time. ^{1}H detection (200 MHz) was applied to map signal intensity. The spatial biofilm distribution, velocity profile, and distribution of the molecular displacement of the water molecules were controlled. T_2 weighting maps allowed spatial investigation of biofilm growth. This research initiated studies in applying MRI results for validation of numerical simulation [166,167].

Fridjonsson et al. [168] monitored biofouling over the membrane module by Earth's magnetic field NMR. Using Earth's magnetic field unlike the previous studies which used a large magnetic field makes this technique more affordable and mobile. T_1 and T_2 relaxation times and total NMR signals were modified to increase specific sensitivity to the stagnant fluid. T_1 and T_2 relaxation times decreased during fouling at the inlet, in the middle, and at the outlet indicating biofouling.

3.3.2. Fourier transform infrared spectroscopy

Fourier transforms infrared (FTIR) spectroscopy has been applied for the characterization of microorganism clusters since 1952 [169]. Molecular stretching and rotation measurement by absorbance of specific wavelengths of the emitted IR light gives the interested matter's chemical composition. Fingerprinting the bacteria with FTIR spectroscopy is based on analyzing the fatty acids, carbohydrates, nucleic acids, and lipopolysaccharide components [170,171]. These are characteristic fingerprints that indicate the biological nature of biofouling on the membrane. This identification can be even at the strain level. However, this method normally is used as a qualitative method, even though it can be used for the quantification of bacteria. Discrimination of viable, injured, and dead bacteria is another capability of this technique [172–174]. Unlike analytical biochemical tests, serological tests, and DNA or RNA-based molecular methods that are invasive and time-consuming, FTIR analysis is economic, fast, and non-destructive. However, variations in spectra can be affected by growth time, temperature, and media [175,176].

Sampling depth limitation [151] and interference with water molecules [152] are other challenges. Distinguishing differences between spectra is difficult due to the overlapping of bands that are emitted by various molecules in EPS, and cell components. Inorganic or organic foulant adsorption on to and penetration into the membrane could be studied by measuring the absorbance intensity of associated stretching bands [177].

Schmitt and Flemming [150] used the second derivative spectrum to distinguish *Pseudomonas putida* and *Pseudomonas fluorescence*. The second derivative spectrum can also be useful to avoid inorganic interference, such as silicates, carbonates, phosphates, and iron interferences in the carbohydrate band.

Donlan et al. [153] applied ATR-FTIR to quantify biofilm associated with *Streptococcus pneumoniae*. The internal reflection element (IRE) substrate was performed by FTIR spectroscopy for online real-time monitoring. An increase in the intensity of the polysaccharide band was observed during biofilm formation relative to the protein amide I and amide II bands. As spectra of bacteria are similar, distinguishing bacteria were not possible by FTIR spectra.

Benavente et al. [154] mapped BSA foulant on the modified membrane by FTIR to investigate membrane fouling propensity. BSA fouling was performed on the polystyrene-polyethylene glycol methacrylate (PEGMA) copolymer modified polyvinylidene fluoride (PVDF) membrane by FTIR mapping of peak intensity for C–H aliphatic (2,876 cm^{-1}), C=O (1,737 cm^{-1}), and N–H (3,300 cm^{-1}) singled general backbone, PEGMA, and BSA, respectively. BSA-associated peak intensity decreased by diblock copolymer modification.

Synchrotron IR spectroscopy is a precise technique to map chemical distribution on the surface with a high signal-to-noise ratio by applying brighter IR than conventional ways [178]. Xie et al. [179] applied synchrotron FTIR to map cross-section spatial fouling distribution on membrane distillation. Combined organic/silica fouling was performed. The silica, humic acid, alginate, BSA, polytetrafluoroethylene (membrane surface), membrane-fouling layer interface were signaled by measuring peak intensity of Si–O (1,116 cm^{-1}), aromatic C (1,750 cm^{-1}), C=O (1,596 cm^{-1}), amid I (1,650 cm^{-1}), and C–F (1,218 cm^{-1}) adsorptions, respectively. Absorbance as a function of position was plotted to generate count plots mapping organic/silica fouling across the membrane for alginate/silica fouling. The C–F bond absorbance for the membrane-fouling layer interface helped to quantify transported silica within the membrane.

Maddela et al. [180] investigated responsible EPS bond peaks of twenty-three different bacteria strain using FTIR in the Ca^{2+} environment. EPS of bacterial strains differed mainly in IR regions that belonged to polysaccharide and protein peaks. Spectroscopic analysis of single-strain biofouling revealed responsible peaks for biofouling as α-1,4-glycosidic bond (920 cm^{-1}), amide II (1,550 cm^{-1}), and uronic acids (1,020 cm^{-1}). The first two peaks were spotted in high and medium-level biofouling. How Ca^{2+} impacts the biofouling is related to the EPS functional groups. Cations had no impact on the biofouling potential low biofouling strains while it decreased the high biofouling strains' biofouling potential. Rahman et al. [181] characterized the chemical composition of a year-fouled seawater RO membrane from the desalination plant. Protein and polysaccharides were identified by amide I, II (1,650; 1,550 cm^{-1}), and C–O (near 1,040 cm^{-1}) stretching bands, respectively.

3.3.3. Raman spectroscopy

Raman spectroscopy is a fingerprinting method based on the rotation and vibration of the functional groups of the molecules in response to the scattered infrared light. Although this technique is more expensive than IR spectroscopy, it does not have a sampling depth limitation (>100 nm) and is also applicable to be used for wet samples compared to FTIR [171,182], unlike FTIR which gives an overwhelming peak at 3,000 cm^{-1} for water. A challenge of Raman spectroscopy is the interference of the membrane itself to the biofilm. Even though typical Raman spectroscopy is useful in chemical analysis of the membrane surface, it is not efficient in the chemical analysis of the fouling layer on the membrane [183]. Hence, Virtanen et al. [184] investigated the applicability of Raman in real-time monitoring of polyethersulphone UF membrane fouling by Vanillin. The variance in the spectral datasets was analyzed by the Principal component analysis (PCA) multivariable analysis technique and the concentration of adsorbed Vanillin over time was successfully acquired. However, using normal Raman is still challenging due to the difficulty in the detection of Raman scattering.

Later Kögler et al. [157] developed an online and real-time surface-enhanced Raman spectroscopy (SERS) sensing technique to identify membrane biofouling. The clean membrane was pre-coated by Au NPs to sense biofouling and eliminate the interfering spectra from the membrane. *Brevundimonas diminuta* bacteria and adenine fouling were investigated separately. It was seen that Au NPs can penetrate the membrane pores and give interfering SERS signals arising from the membrane composition. These interfering signals were eliminated and excluded from Raman spectra according to results obtained from CLSM, Raman, and scanning-microscope results of bare membranes. No significant differences were observed between online and offline tests, which approved the robustness of this method.

In SERS, particles coated on the membrane should not have a toxic effect on the biofilm. Ag NPs toxicity on the bacteria at SERS was elucidated by Cui et al. [185] in comparison to the non-toxic Au NPs. SERS spectra variation was observed by the toxicity of the Ag NPs on the bacteria. So considering this point, Ag NPs could be utilized as an antiseptic coating on the membranes and at the same time could have a lateral role as a signal enhancer in SERS.

Cui et al. [158] applied SERS to investigate layer-by-layer chemical constitutes variation during biofouling and cleaning. *B. diminuta* bacterial biofouling was performed on the RO membrane. SERS measurement and SEM visualization were acquired at different stages of biofouling for biofouling determined by the flux variation. SERS spectra intensity was insensitive to biofilm thickness and remained almost unchanged at the early stages because SERS only provides information on the chemical composition of substances nearby the Au NPs. Membrane cleaning results based on SERS measurements revealed that surfactant SDS cleaning was more effective for lipids than other

components and also the remained DNA and protein contributed to the irreversible biofouling.

Enabling online monitoring, early-stage biofouling detection, and no risk of sample manipulation were the main advantages of the SERS technique. However, nanoparticle (NP) dissociation under the cross-flow velocity, the probe-focusing problem underwater pumping [157], limited analysis domain to the nearby substances of metallic NPs [158], difficulties in metallic nanoparticle coating [157] limits the application of the SERS technique.

3.3.4. X-ray photoelectron spectroscopy

X-ray photoelectron spectroscopy (XPS) is used for analyzing the chemical composition of membrane surfaces, biofilm layers, and for evaluating the cleaning efficiency of membranes [69,70]. In this method, an illuminated X-ray on the specimen ejects electrons from a specific orbital under a high-vacuum atmosphere. The kinetic energy of the photo-ejected electrons gives information about binding energy. The energy of the photo-ejected electrons is attenuated as reaching to the top. The sampling depth is three times that of the inelastic mean free path of electrons in the specimen. So, the sampling depth will be around 3–10 nm for AlK_{α} radiation. In this depth, 95% of the photoelectrons are scattered. Polysaccharides, proteins, another hydrogen, and carbon-containing compounds can be acquired by quantitative analysis of the specimen surface.

Khan et al. [69] analyzed the chemical composition variation of the RO membrane after biofouling and physical cleaning. Due to the EPS layer formation by the fouling, carbon and nitrogen content decreased while the oxygen increased. This variation in elemental composition perhaps is because of EPS content with a higher O/C ratio. After cleaning the surface of the aliphatic molecule modified membrane had the lowest O/C ratio due to the lower EPS accumulation while hosting higher cells.

3.3.5. Electrochemical impedance spectroscopy

Electrochemical impedance spectroscopy (EIS) is a promising technique for in-line and non-destructive identification and characterization of membrane and fouling layers. Building up layers on the membrane surface causes decreases in the intrinsic conductivity of the membrane. Insights on fouling layer type and its extent can be acquired by feedback-based measurement of phase shift in sinusoidal voltage and current after directing a low amount alternating current (AC) with a specific frequency to the membrane. The feedback measurement gives information about the amount of resistance, a charge carrier should sustain during its transport from the electrolyte to the electrode [186]. Each layer of fouling, membrane, etc. could be modeled as a dielectric circuit by the Maxwell-Wagner model [187]. The layers are in series with their resistivity (R) and capacity (C). Generally, four types of plots are investigated including (1) conductance-frequency plot (2) Nyquist plot (3) capacitance-frequency plot, and (4) TMP-time plot. Dispersion of conductance and capacitance with frequency reflects the existence of different substances [188]. Nyquist plots 'negative imaginary impedance (related to electrical capacitance) against real impedance (related to electrical capacitance) for three frequency regions of solution layer with high frequency, membrane layer with mid-frequency, and diffusion-polarization layer with low frequency. TMP-time plot has been employed comparatively a long with EIS to show early-stage detection and high efficiency of EIS.

The high sensitivity of electrochemical parameters in EIS helps to diagnose fouling at its early stages and identify foulant type in the membrane process. Assessing membrane cleaning efficiency is another capability of EIS. This technique has been applied in analyzing the fouling and cleaning of UF [189], NF, RO [190,191], and ion-exchange membranes [192,193].

Park et al. [193] investigated conductance and capacitance dispersions with the frequency that arose from BSA fouling of the anion-exchange membrane. The impedance of the solution for both unfouled and fouled membranes in the solution was subtracted. A decline in conductance and capacitance was observed by BSA fouling. Later in 2006, Park et al. [192] investigated current-voltage and EIS by offsetting AC. Current-voltage curves indicated a reduction in the total resistance of the ion-exchange membrane due to the BSA fouling layer. In EIS analysis, the BSA fouling layer acted as an additional capacitive loop. Increasing current density increased water dissociation and EPS layer density. Protons from water dissociation neutralized the negatively charged BSA layer, in turn, a decline in resistance occurs. Kavanagh et al. [190] investigated conductance and impedance sensitivity for fouling on seawater RO membrane and impedance showed great sensitivity for fouling which dramatically increased at frequencies below 100 Hz even by a small amount of divalent slats precipitation.

Sim et al. [191] investigated silica and BSA fouling of the RO membrane. Silica concentration polarization caused Nyquist plots to shift to the leftover time indicated a decline in overall conductivity. By further silica fouling a stagnant layer formed under the flowing layer which inhibited back diffusion of salt ions and increased the overall conductivity by cake enhanced concentration polarization (CECP). In BSA fouling, Nyquist plots shifted to the right, unlike silica. This different behavior originates from the different nature of foulants. Nyquist plots identified fouling with high sensitivity while for TMP it took 15 h to respond significantly to fouling.

A similar experiment to the aforementioned research was carried by Cen et al. [194]. Capacitance measurement at low frequency (~1 Hz) was more sensitive than both conductance and flux monitoring. Similarly, the capacitance value of BSA and silica at low frequency (~1 Hz) changed differently due to their different natures. BSA capacitance at low frequency declined while this value for silica increased.

Ho et al. [195] investigated fouling and chemical cleaning by monitoring the normalized real part of the impedance ($N\text{-}Z_{DP}$) in an RO treatment field trial study. Between cleaning periods, $N\text{-}Z_{DP}$ was increased due to the non-conductive matter accumulation and then decreased via CECP phenomena. $N\text{-}Z_{DP}$ was suggested as a good indicator for assessing the efficiency of different cleaning agents and strategies.

EIS had not been applied to investigate membrane biofouling until 2016. Ho et al. [162] investigated membrane biofouling mechanisms by EIS. Normalized conductance

of diffusion polarization (N-G_{DP}) was monitored during *Pseudomonas aeruginosa* biofouling. N-G_{DP} reached its maximum point at 1.5 d followed by a decline as biofouling continued. However, N-G_{DP} showed only an increasing trend during dead bacteria and nutrient fouling. This difference was related to the two stages of biofouling as bacterial adhesion and EPS layer production. This interpretation was supported by the results of CLSM, TMP, and dead bacteria-alginate mixture fouling. Alginate was applied to mimic the EPS. The increasing concentration of EPS changed the N-G_{DP} trend from an increasing trend to decreasing trend.

Sengur-Tasdemir et al. [187] compared BSA fouling propensity of polyethersulfone (PES), polysulfone (PS), and PVDF UF membranes by EIS. Charge-transfer resistance increased for all the membranes after BSA fouling. The lowest charge-transfer resistance was observed for the PVDF membrane which unanimously the highest flux recovery rate after cleaning BSA fouled membrane has resulted in the PVDF membrane. Moreover, Genceli et al. [196] applied EIS for the first time in the nanocomposite hollow fiber membrane to analyze the effect of carboxylated multiwall carbon nanotube (MWCNT) incorporation on the performance and fouling property of membranes. Double-layer capacitance arose by increasing the diameter and concentration of MWCNT. By decreasing the outer diameter of MWCNT at higher concentrations lessened the double-layer capacitance of the membrane. The diminishing double-layer capacitance of the membrane was reflected in the enhancing flux recovery rate after cleaning the BSA fouled membrane.

3.4. Techniques for studying microbial community in the biofilm

Microbial analysis techniques have been applied to get insights into the quantities of target biofoulant in biofilm, bacterial species forming the biofilm, and how these bacteria evolve and space. Most common related techniques including denaturing gradient gel electrophoresis (DGGE), terminal restriction fragment length polymorphism (T-RFLP), fluorescence in situ hybridization (FISH), real-time polymerase chain reaction (PCR), and next-generation sequencing (NGS) are discussed below and briefly listed at Table 4 along with their strength and limitations.

3.4.1. Culture-dependent method: isolating bacteria directly from the biofilm

Many studies have employed cultivation methods as a means of investigating the microbial community structure of membrane biofilms [203]. The culture-dependent method involves isolating the bacteria from the biofilm before enriching it in a suitable culture. One of the disadvantages of this technique is that the outcomes are not necessarily reflective of the diversity of the biofilm microbial communities. This is because it is only possible to cultivate a small fraction of the total bacterial community under standard laboratory conditions in oligotrophic systems. It is possible to address some of the shortcomings associated with the cultivation methods that are available through the application of molecular-based approaches. For example, rDNA or rRNA-based methodologies can generate meaningful insights into the composition and diversity of microbes while also semi-quantitatively defining the abundance of these microbes in natural and manmade environments [204,205]. By combining these molecular techniques with cultivation approaches, it is possible to adopt a polyphasic approach that can generate more meaningful insights into the structure of the microbial community structure and how it functions in a given manmade or natural environment.

Table 4
Comparison of the function and problems of the spectroscopic techniques in the membrane biofouling analysis in terms of advantages and limitations

Methods	Advantages	Limitations	References
DGGE	- Enables direct comparison of total community composition at a glance and identification of individual components by excision and sequencing of bands	- Probability of non-reproducible preparation of denaturant gels with chemical denaturing agents	[197]
T-RFLP	- Enables making direct reference to the sequence database	- Time-consuming, labor-intensive, often the use of radioactive materials - Probability of interference of nonspecific PCR products to the analysis	[198]
FISH	- Allows in situ localization and the study of the spatial organization of cells as they occur in their natural habitat or biofilm - No needs for cell cultivations - No need for alive cells	- Complex process - Difficult to count total numbers in probe-stained clusters of cells	[199]
Real-time PCR	- Quantifies interest gene in 96 or 384 well plate formats in a shorter time	- Multiple-targeting. 5-flex (5 colors) is possible	[199]
Next-generation sequencing	- Rapid - 1,000,000 high-quality reads per run	- Limitation in the read length	[200–202]

3.4.2. Understanding microbial community structure by molecular techniques in the biofilm

3.4.2.1. Cloning and sequencing

Through the application of cloning and sequencing techniques, it is possible to isolate large quantities of genes or chromosomal fragments. Besides, cloning can be employed to identify and characterize any microorganisms that exist in a diverse environment. DNA fragments can be produced in two ways: after digestion with the restriction enzymes of DNA extracted from a sample, or after polymerase chain reaction (PCR) or reverse transcription-PCR (RT-PCR) [206]. 16S rRNA clone library-based analysis also represents a useful approach through which the analysis of microbial diversity and biofilm structure analysis can be conducted [207].

Although cloning is also not without bias, the use of 16S rRNA gene sequences to study new microorganisms has become common. It is not possible to conduct a sufficient investigation into environmental microbial communities without 16S rRNA sequence data. Bereschenko et al. [208] employed 16S rRNA clone libraries as a means of developing insights into the composition, origin, and structure of the biofilm found in several portions of an industrial RO membrane. Their findings revealed that the relative wealth of the various species identified in the mature biofilm varied from those present in feed water. They concluded that this was indicative of the fact that the biofilm actively developed on RO membrane sheets as opposed to being introduced via the concentration of bacteria that were present in the feed water. The researchers also concluded that biofouling of the membranes in RO installation could be attributed to the members of the genus *Sphingomonas*. Most of the biofouling analysis experiments on the membrane have been carried by *E. coli* as a model bacterium. Saffarimiandoab et al. [58] isolated and identified five different marine biofoulant bacteria to model the aquatic environment in a more realistic way for biofouling experiments. Isolated biofoulant marine bacteria from a biofouled RO membrane were identified by amplifying and partial sequencing of the 16S rRNA gene. Gene sequences were compared with 16S rRNA clone databases and the following genera were revealed: *Shewanella*, *Vibrio*, *Oceanimonas*, *Cobetia*, *Pseudoalteromonas*. Ziegler et al. [209] employed 16S rRNA gene sequences by a curated taxonomy and fluorescent in situ hybridization to study the change in the biofilm community over the maturation. According to their findings, the biofilm community gets similar to the microbial community of the bulk water. Hence, it was concluded that the microbial population of mature biofilm can be identified based on the bulk water microbial diversity.

3.4.2.2. Next-generation sequencing

The parallel sequencing method is relatively new to molecular biology that has exhibited significant potential in the field of environmental analysis. The various next-generation sequencing systems that are available include 454 Life Sciences (Branford, CT), HeliScope system (Helicos Biosciences, Cambridge, MA), Polonator system (Dover Systems, Salem, NH), Solexa system (Illumina, San Diego, CA), and SOLID system (Applied Biosystems, Carlsbad, CA). Each system has been found to deliver high data output and various length capacities. Through the application of next-generation sequencing technologies, scientists and researchers have been able to characterize the molecular diversity of microbial communities. Also, next-generation sequencing technologies facilitate the functional analysis of bacterial and archaeal communities. However, one of the drawbacks to deep-sequencing-based technologies is that they rely on comprehensive bioinformatics databases and need sophisticated software to effectively process the data associated with sequencing. Next-generation sequencing can be considered a representative, sustainable and efficient method of analysis.

Many of the existing studies that involved next-generation sequencing have been relatively restricted due to the limited applicable range for the bacteria community and the fact that the research did not employ deep sequencing. These limitations resulted in partial and, therefore, contradicting results. In one study, Mikhaylin and Bazinet [210] employed next-generation sequencing to assess the bacterial abundance, diversity, and community composition of RO membrane biofouling layers that were formed under various hydrodynamic shear rates. The findings of this research revealed that the variations in the shear rates applied during the desalination processes had a significant impact on the RO-membrane biofilm. Specifically, a direct relationship between the shear rate and the microenvironment that emerged was found, and that this microenvironment ultimately mediates selection for different bacterial communities.

Pyro-sequencing is a method of next-generation sequencing that can identify microbes via a high-throughput screening approach. Recent studies [200,206] have demonstrated that the use of pyro-sequencing in membrane studies increased the sensitivity of community analysis compared to denaturing gradient gel electrophoresis (DGGE) of 16S rRNA clone library analyses. Also, it facilitated a more in-depth investigation into microbial species [200,206]. Jeong et al. [211] employed 454-pyrosequencing technologies to develop insights into the microbial communities that are responsible for membrane biofouling in MBR and removing organic compounds in submerged membrane adsorption bioreactors. Bacterial community analysis showed that α-proteobacteria were found to be principal microorganisms on the biofilm layer of the fouled seawater RO membrane. *Firmicutes*, *Actinobacteria*, *Planctomycetes*, and *Bacteroidetes phyla* were also identified as biofoulant bacteria.

Yavuztürk-Gül et al. [201,202] used the Illumina sequencing method to determine the impact of Quorum Quenching (QQ) bacteria on the relative abundance of the microbial community in MBR. This approach enables a better understanding of membrane biofouling and microbial relationships between QQ bacterium *Bacillus* sp. T5 and bacterial community structures in MBRs. According to the results, the QQ process caused structural variations in the microbial community and the interaction between *Bacillus* sp. T5 and the indigenous bacterial population are critical to the performance of the system.

3.4.3. Quantification of microbial communities

3.4.3.1. Real-time quantitative PCR

Real-time quantitative PCR (qPCR) is a highly reproducible and sensitive screening technique that is possible to monitor the phylogenetic and functional evolution of genes in a variety of different experimental and environmental conditions across special and temporal scales quantitatively. The quantitative data that is produced during the qPCR technique can be employed to compare changes in the abundances of genes and/or the levels of gene expression with modifications in the biological activities and features [200]. qPCR data sets are described in accordance with the abundance of specific bacteria or genes for the completion of other quantitative environmental data sets. This provides insights that facilitate an understanding of how certain microbial and functional groups within the ecosystem contribute to that system and the roles they play within it. It is possible to combine reverse transcription (RT) analyzes with qPCR methods in RT-qPCR assays to create a powerful tool that can quantify gene expression and the relationships between biological activity and ecological function.

While qPCR is not commonly employed to analyze biofilm in membrane systems, it represents a very effective method for analyzing the microbial consortia of biofilms. For example, Al Ashhab [212] investigated the influence of feed-water shear rate during RO desalination on biofouling on the composition of the microbial in biofilm. A microbial community developed on RO-membrane biofilm was profiled through desalination effluent of tertiary wastewater. Experiments were conducted in a lab-scale system by applying low, medium, and high shear rates. Researchers found that bacterial diversity was found highest when a medium shear rate was applied. At this medium rate, *Betaproteobacteria* was found dominant in RO membrane biofilms. However, under lower and higher shear rates, α- and γ-Proteobacteria dominated the biofilm. In addition, RO-membrane biofilms that were developed under high shear rates also contained *Deltaproteobacteria*. The results of this research indicate that the abundance, composition, and structure of RO-membrane biofilm differs following the shear rate applied.

3.4.3.2. Fluorescence in situ hybridization

Fluorescence in situ hybridization (FISH) is a set of powerful techniques that are employed to detect the positions of genes on chromosomes. It involves microscopic analysis of defined groups of bacteria by a fluorogenic oligonucleotide (or probe) targeting small subunit ribosomal RNA (SSU rRNA) molecules inside cells. The process involves several steps. First, chemical fixatives are employed to fix microbial cells. These cells are then hybridized on a glass slide or in a solution with oligonucleotide probes under optimal conditions. Oligonucleotide probes are typically 15–25 nucleotides and a fluorescent dye is employed to label them covalently at their 5′end. rRNA targets oligonucleotide probes without cultivation can help to determine the composition and number of bacteria. One of the biggest advantages of FISH is that it does not involve a PCR approach. As such, it is not subject to the biases that are typically associated with the PCR procedure. This means that it is particularly useful for validating the results of a microbial community with other PCR-based molecular techniques, such as DGGE and 16S rRNA clone library analyses. For example, in one study, Chen et al. [207] examined the microbial communities of membrane biofilms that occurred in two full-scale water purification processes. They employed bacterial cultivation, 16S rDNA clone library, and fluorescence in situ hybridization techniques to characterize microfiltration (MF) and RO membranes. All methods revealed that α-*Proteobacteria* was the largest microbial fraction in the samples, followed by γ-*Proteobacteria*. Several additional studies have been employed FISH for biofilm analysis [199,213].

FISH represents a valuable research tool that can be employed to identify and quantify the specific bacteria that exist in a given microbial community. It can also significantly enhance understanding of the spatial interactions that exist within complex microbial communities. Besides the advantages of the FISH technique, one of the significant issues with FISH analysis is that standard fixation protocols cannot be used to permeabilize bacterial and archaeal cells using oligonucleotide probes. Furthermore, to use FISH, scientists need to have an existing understanding of the ecosystem that is the subject of investigation and the microorganisms that reside within it. In addition, it is not always possible to develop a specific probe for a given group of microorganisms [214].

3.4.4. Fingerprinting techniques

Unlike cloning and sequencing techniques, fingerprinting can be readily scaled to allow the rapid analysis of large samples, including duplicates. Fingerprinting produces data that can be quantitatively or semi-quantitatively analyzed to assess the relative abundance of various members of the community. Denaturing gradient gel electrophoresis and thermal restriction fragment length polymorphism will be investigated in this respect.

3.4.4.1. Denaturing gradient gel electrophoresis

Denaturing gradient gel electrophoresis (DGGE) is a form of electrophoresis in which nucleic acids migrate in a chemical gradient according to their gradient gel GC content. DGGE is based on the melting temperature of double-stranded DNA fragments. Even in the case of a single-nucleotide substitution, fragments can melt at different temperatures. A fragment can be produced by adding the GC-rich tail (GC-clamp) to the primers for amplification. This fragment will partially melt when it is electrophoresed in a denaturing gradient polyacrylamide gel [215]. The GC clamp will remain double-stranded, and the resulting fork-like structure will cause the fragment to stop migrating. It is also possible to detect mutations from base-pair substitutions/deletions because these mutations will occupy different positions in the gel.

DGGE fingerprinting has been proven to represent a reliable method of examining the spatial and temporal changes that take place in microbial communities. In addition, DGGE

can represent a very valuable technique for supervising complex communities by allowing researchers to focus on phylotypes that are affected by environmental changes in terms of availability and relative frequency. However, DGGE is unable to detect minor community components that represent less than 1% of the community [215].

Several researchers have utilized DGGE to examine changes in the microbial communities of biofilms [197,216,217]. For example, Ivnitsky et al. [116] studied the structure of biofilm along with its microbial diversity developed at various temperatures and locations on NF membranes. They analyzed the composition of the community through the use of a sequence analysis of the 16S rRNA gene fragments from dominant bands in combination with polymerase chain reaction–denaturing gradient gel electrophoresis (PCR-DGGE).

3.4.4.2. Terminal restriction fragment length polymorphism

Terminal restriction fragment length polymorphism (T-RFLP) is another fingerprinting technique. This approach produces patterns of microbial community diversity that can be readily interpreted. These patterns can be useful for studying the relative diversity and abundance of microbial communities and can be used in combination with meta-community sequencing-based approaches [211]. T-RFLP employs PCR through a technique in which one of the two primers is fluorescently labeled at the 5′ end for the amplification of a specific region of the 16S rRNA gene or functional genes. After the amplification, products of PCR are cleaved with a site-specific restriction endonuclease to obtain a specific product from a single microorganism or the genetic fingerprints of microbial communities [211]. T-RFLP represents a powerful tool that is capable of assessing the diversity of complex microbial communities. Also, it can facilitate an efficient, low-cost, and rapid comparison of the diversity and community structure of various water systems. In addition to being half-quantitative, T-RFLP is often combined with 16S rRNA clone library analysis since it does not allow phylogenetic identification. However, this is not its disadvantage. In particular, it exhibits PCR bias and a lower resolution than many of the available alternative methods.

Jeong et al. [211] employed a T-RFLP-based community assessment to characterize the community composition by PAC addition in MBR and to correlate with the composition to assess the system performance. Following the addition of the powdered activated carbon (PAC), the composition of the bacterial community was significantly differentiated. As such, the data produced via this research indicates that MBR performance can be improved through the addition of PAC. Because PAC leads to the development of different bacterial species that control assimilable organic carbon (AOC) and the associated biofouling on the membranes. Piasecka et al. [218] monitored the richness of bacterial species found on the surface of membranes that are treated with different NaOCl concentrations according to the number of T-RFs peaks obtained from the T-RFLP profile. And Liu. [198] employed a polyphasic approach to examine the biofilm community structure of a biofouled RO membrane. The dominant phylotypes retrieved during this study were related to the *Rhizobiales* order, a bacteria group that has not previously been associated with membrane biofouling. They concluded that *Rhizobiales* organisms are of ecological significance within membrane biofilm communities under both aerobic and anoxic conditions and that they may cause biofouling in membrane separation systems.

3.5. Other methods used for biofouling determination

3.5.1. Contact angle

Contact angle measurement has been applied to measure the variation of membrane hydrophilicity after fouling, cleaning, and free energy of interaction between foulant and membrane surface. Water contact angle (CA) after fouling depends on the foulant and membrane interaction property. Cho et al. [219] characterized natural organic matter fouled UF and NF membranes.

Khan et al. [69] investigated physical cleaning efficiency in retaining the initial water contact angle of the biofouled RO membrane. WCA for clean RO membrane and cleaned membrane after biofouling was reported as 54 and 80 respectively. Zhao et al. [220] investigated WCA variation of NF membrane after condition layer deposition and further biofouling. WCA of NF membrane decreased from 66.7 down to 64.0, 30.2, 55.8, and 41.9 by no organic matter, sodium alginate, BSA, and humic acid conditioning. Unconditioned and conditioned membranes were biofouled with *Pseudomonas aeruginosa*. WCA values of biofouled membrane were reported as 23.4, 40.6, 41.2, 54.3 on no organic matter, sodium alginate, BSA, humic acid conditioned membranes.

3.5.2. Oxygen decrease rate

The application of transparent luminescent planar O_2 optode sensor can be applied in early and non-destructive biofouling diagnosis and monitoring by mapping oxygen decrease rate (ODR) and distribution [221]. Spatial and quantitative biofilm distribution analysis has been studied by combining O_2 optode sensing and membrane cell imaging. Being a user-friendly imaging technique and having small equipment made this technique interesting for research and industrial purposes. However, as the main drawback, the role of EPS as a main component in biofouling cannot be assessed by this technique. Another disadvantage is that ODR measurement is limited only to a thin layer at the bottom of the biofilm on the membrane and not the whole biofilm volume [222]. O_2 optode sensing is applicable only for aerobic fluid conditions while anaerobic pH or CO_2 should be sensed [223].

Staal et al. [224] applied O_2 optode sensing to image the spatial distribution of oxygen at the base of membrane biofilm and investigated its applicability for applying in membrane fouling simulator. Later, Prest et al. [222] studied monitoring time and space resolved O_2 consumption rate and linked them to flow and biomass distribution maps in membrane fouling simulator. O_2 concentration decreased by either thick biomass formation or limited mass transfer. Due to biomass detachment, O_2 concentration on day 11 was found higher than day 9 and day 10.

Farhat et al. [223] investigated the applicability of oxygen sensing optodes in early detection and spatial distribution monitoring of membrane biofouling. Spatial resolved ODR was measured under cross-flow and stop-flow operation modes. A location where ODR increased compared with qualitative direct imaging using rhodamine dye. Higher ODR was linked to the higher bacterial population. Stop-flow imaging resulted in better biofouling diagnosis in terms of early detection while biomass detachment was observed in this operating mode. In another work, Farhat et al. [225] investigated biofouling development on RO membrane 10°C, 20°C, and 30°C. Biofilm activity was analyzed by measuring ODR from luminescence intensity imaging of O_2 concentration. Biofilm activity was lowest at 20°C and for 10°C, it was slightly higher than 30°C. The lowest biofilm activity at 20°C was cleared by CLSM of biofilm in which the lowest bacterial cell to EPS ratio was observed at 20°C. Different biofilm structure was related to limited nutrient and oxygen consumption. Thin layer biofilm, higher bacterial cell to EPS ratio, and higher nutrient diffusion enhanced biofilm activity at 30°C. CLSM and luminescence intensity imaging of O_2 concentration had different capabilities but they were complementary in clearing biofouling behavior. Farhat et al. [226] also analyzed the impact of crossflow velocity on biofilm activity and biofilm spatial heterogeneity at the entrance and outlet of the membrane fouling simulator. Higher biofilm heterogeneity is identified by a higher standard deviation in oxygen concentration. Higher biofilm heterogeneity was observed for the inlet than the outlet. The extended area for heterogeneous biofilm is observed by decreasing crossflow velocity. There is a tradeoff between bacterial adhesion and bacterial detachment in higher crossflow velocity. Higher ODR with lower crossflow velocity was the result of balancing bacterial adhesion, growth, and detachment. The findings gave helpful insight into finding and optimum operational conditions and biofouling control strategies.

Besides luminescence intensity imaging of O_2 concentration, specific oxygen consumption rate (SOCR) is calculated from point measurement of oxygen concentration can be applied in in-situ and early membrane biofouling detection [243,244]. Kappelhof et al. [228] carried three experiments monitoring biofouling in RO. According to the authors, SOCR measurement enables decreased biofouling detection time twice compared to normalized pressure difference measurement.

3.5.3. Zeta (ζ) potential

Membrane surface charge has a direct effect on the adsorption of organic and inorganic charged matters. Hence, surface Zeta (ζ) potential analysis, as an electrokinetic property, has been carried in determining membrane propensity for fouling.

The streaming potential is the most capable technique among the other available techniques for zeta-potential measurement where electrolytes flow tangentially from the surface of the membrane. However, in the case of membranes electrolyte direction is perpendicular to the surface and consequently, the potential is obtained due to the electrolyte going through the pores. An electrical double layer would be formed as the electrolyte convective flow passes through the pore, which forms two convective currents in opposite directions. From the theoretical view, the zeta potential can be acquired from the streaming potential by the Helmholtz–Smoluchowski equation [229], Eq. (1):

$$\zeta = \frac{\eta K}{D\varepsilon_0}\frac{\Delta E}{\Delta P} \tag{1}$$

The ζ is the apparent zeta potential, D is the dielectric constant of the fluid, ε_0 the permittivity, η, and K stand for the viscosity and conductivity of the fluid, and $\Delta E/\Delta P$ is the streaming potential across the membrane due to pressure gradient.

Measuring the zeta-potential variation by fouling over different pH can give information on the adsorption mechanism of foulant. In BSA fouling of the membrane, Nystrom et al. [230] investigated water flux and zeta potential variation of polysulfone membrane in the case of BSA fouling. The zeta potential of BSA fouled membrane shifted towards a positive region from a slightly negative value at pH of 5.1 while BSA with an isoelectric point of 4.8 is expected to have a neutral or slightly negative surface charge. Hence, BSA adsorption takes place by hydrophobic interactions rather than electrostatic interactions at a pH of 5.1 which considerable flux decline was observed.

The zeta potential of the cleaned membrane after fouling can give information about membrane recovery, but cleaning with high pH may cause membrane damage and it would expose more negative groups, and consequently, more negative zeta potential would occur. In other efforts [231,232], streaming potential variation of − 3 mV charged membrane fouled with − 30 mV charged latex suspension was analyzed. Although foulant had a more negative charge than the membrane, the absolute value of the streaming potential decreased. This result was related to the behavior of the latex suspension as the concentration layer does not act as a cake layer, which leads to a decrease in the electrokinetic flux and subsequent lowering of the absolute value of the streaming potential.

In time, in-situ membrane fouling monitoring with streaming potential measurement techniques was emerged [233–235]. These techniques have been coupled with flux monitoring for verification over fouling time. In ex-situ mode, the fouled membrane was removed from the cell membrane for further streaming potential variation measurement. But later, in-situ monitoring protocols have been developed for trans-membrane streaming potential monitoring during fouling. Transmembrane zeta-potential variation and flux decline have been related to each other in studies of the zeta potential behavior. This is crucial especially in the biofouling study where the microorganism containing the EPS layer undergoes compression during filtration which leads to erroneously acquired streaming potentials. By considering no ion rejection, smaller pores than the foulant and incompressible cake layer, the measured electrical potential of the fouled membrane are in linear relation with permeate flux. The pressure drop is independent of the applied pressure. Zeta potential can be calculated by measuring the slope.

Teychene et al. [234] developed a new protocol for in-line electrical potential monitoring during cake layer formation. The fouling was tried by spherical latex particles. In in-line mode, electrical potentials measurements were done at constant pressure while in classical mode electrical potentials measurements were done at different pressure steps. Firstly, an electrolyte was passed through the membrane to achieve membrane-electrolyte electrochemical equilibrium. Afterward, latex suspension was filtered to form a cake layer. Finally, the new electrical potential was measured by the passage of the electrolyte at the same pressure.

Recently, Jia et al. [235] monitored zeta-potential variation and flux decline of the PVDF hollow fiber membrane during yeast solution fouling. Fouling was performed at a pH of 6.1 in which the zeta potential of clean membrane and yeast solution was –6.1 and –18.5 mV, respectively. Three different membrane fouling phases were observed based on zeta potential response inline monitoring. Firstly, the rapid decrease observed in the zeta-potential was linked to pore blockage, electrostatic repulsion between membrane and yeast, double electric layer formation, and concentration polarization; secondly, the gradual decrease in the zeta-potential was related to the inhibition of pore blockage with cake layer formation; and finally, the zeta-potential stabilization occurred due to layer compression.

4. Concluding remarks

This study, first, provided detailed insights on the biofouling mechanisms in various membrane processes. Then the established tools and techniques for biofouling diagnosis, monitoring, and biofilm characterization were critically reviewed. Even though various efforts have been tried to develop theories on mechanisms of biofouling, it is not still fully resolved; especially, rising unconventional, novel or hybrid membrane processes have made it more complex. Biofouling remained the most challenging issue of membrane technology in water and wastewater treatment. Each of the reviewed techniques in this study on microscopic, spectroscopic, and biological techniques for analyzing biofouling has different capabilities, strengths, and weaknesses as listed in the given tables. Microscopic techniques' primary aim is the investigation of biofilm structure and cannot resolve the chemical composition of biofilm except CLSM which requires expensive fluorescent staining. Besides, artifact and sample damage is the most concerned common issue associated with the microscopic technique. Among spectroscopic techniques, EIS is a promising technique for "in-line" and "early-stage" biofouling detection and monitoring techniques with relatively higher sensitivity. Biological techniques are more passive and are suitable for fingerprinting and characterization of microbial communities. These advantages and disadvantages lead the researchers to devise hybrid techniques for better analysis. However, most of these techniques still are practiced in the laboratory and on industrial scales instead usually transmembrane pressure and system performance monitoring, membrane autopsy, and feed water analysis are employed for alarming biofouling initiation. Even though spectroscopic and microscopic techniques with "in-line", "non-destructive", and "early-warning" abilities have shown to be promising, upscaling these techniques for industrial application is still under development. In addition, most of the lab-scale researches were performed with synthetic feed solution, while to acquire more realistic results, it is crucial to apply real feed solution in experiments. Regardless of the lack of commination between research and industrial communities, this gap between the research efforts and industrial needs probably relates to the diverse and complex nature of biofouling which requires developing site-specific biofouling diagnosis and monitoring techniques.

Acknowledgment

The authors are grateful to TUBITAK (The Scientific and Technological Research Council of Turkey) for their financial support under the grant (Project No:111Y356).

References

[1] H.-C. Flemming, Reverse osmosis membrane biofouling, Exp. Therm. Fluid Sci., 14 (1997) 382–391.
[2] H.-C. Flemming, J. Wingender, The biofilm matrix, Nat. Rev. Microbiol., 8 (2010) 623–633.
[3] R. Valladares Linares, L. Fortunato, N.M. Farhat, S.S. Bucs, M. Staal, E.O. Fridjonsson, M.L. Johns, J.S. Vrouwenvelder, T. Leiknes, Mini-review: novel non-destructive *in situ* biofilm characterization techniques in membrane systems, Desal. Water Treat., 57 (2016) 22894–22901.
[4] L.N. Sim, T.H. Chong, A.H. Taheri, S.T.V. Sim, L. Lai, W.B. Krantz, A.G. Fane, A review of fouling indices and monitoring techniques for reverse osmosis, Desalination, 434 (2018) 169–188.
[5] W. Guo, H.-H. Ngo, J. Li, A mini-review on membrane fouling, Bioresour. Technol., 122 (2012) 27–34.
[6] T. Nguyen, F. Roddick, L. Fan, T. Nguyen, F.A. Roddick, L. Fan, Biofouling of water treatment membranes: a review of the underlying causes, monitoring techniques and control measures, Membranes (Basel), 2 (2012) 804–840.
[7] R.A. Al-Juboori, T. Yusaf, Biofouling in RO system: mechanisms, monitoring and controlling, Desalination, 302 (2012) 1–23.
[8] H. Maddah, A. Chogle, Biofouling in reverse osmosis: phenomena, monitoring, controlling and remediation, Appl. Water Sci., 7 (2017) 2637–2651.
[9] X. Du, Y. Shi, V. Jegatheesan, I.U. Haq, A review on the mechanism, impacts and control methods of membrane fouling in MBR system, Membranes (Basel), 10 (2020) 24, doi: 10.3390/membranes10020024.
[10] Y. Chun, D. Mulcahy, L. Zou, I.S. Kim, A short review of membrane fouling in forward osmosis processes, Membranes (Basel), 7 (2017) 30, doi: 10.3390/membranes7020030.
[11] W. Chen, C. Qian, K.-G. Zhou, H.-Q. Yu, Molecular spectroscopic characterization of membrane fouling: a critical review, Chem, 4 (2018) 1492–1509.
[12] F. Saffarimiandoab, B. Yavuzturk Gul, R. Sengur Tasdemir, S. Erkoc Ilter, S. Unal, B. Tunaboylu, Y.Z. Menceloglu, I. Koyuncu, A review on membrane fouling: membrane modification, Desal. Water Treat., 216 (2021) 47–70.
[13] H.-C. Flemming, J. Wingender, U. Szewzyk, P. Steinberg, S.A. Rice, S. Kjelleberg, Biofilms: an emergent form of bacterial life, Nat. Rev. Microbiol., 14 (2016) 563–575.
[14] B. Bhushan, Bio- and Inorganic Fouling, Springer, Cham, 2016, pp. 423–456.
[15] R. Gubner, I.B. Beech, The effect of extracellular polymeric substances on the attachment of *Pseudomonas* NCIMB 2021 to AISI 304 and 316 stainless steel, Biofouling, 15 (2000) 25–36.
[16] S.R. Suwarno, S. Hanada, T.H. Chong, S. Goto, M. Henmi, A.G. Fane, The effect of different surface conditioning layers on bacterial adhesion on reverse osmosis membranes, Desalination, 387 (2016) 1–13.

[17] Z. Adamczyk, P. Weroński, Application of the DLVO theory for particle deposition problems, Adv. Colloid Interface Sci., 83 (1999) 137–226.
[18] M.C.M. van Loosdrecht, A.J.B. Zehnder, Energetics of bacterial adhesion, Experientia, 46 (1990) 817–822.
[19] H.H.M. Rijnaarts, W. Norde, E.J. Bouwer, J. Lyklema, A.J.B. Zehnder, Reversibility and mechanism of bacterial adhesion, Colloids Surf., B, 4 (1995) 5–22.
[20] S. Ishii, S. Miyata, Y. Hotta, K. Yamamoto, H. Unno, K. Hori, Formation of filamentous appendages by *Acinetobacter* sp. Tol 5 for adhering to solid surfaces, J. Biosci. Bioeng., 105 (2008) 20–25.
[21] S. Ishii, H. Unno, S. Miyata, K. Hori, Effect of cell appendages on the adhesion properties of a highly adhesive bacterium, *Acinetobacter* sp. Tol 5, Biosci. Biotechnol. Biochem., 70 (2006) 2635–2640.
[22] S. Ishii, J. Koki, H. Unno, K. Hori, Two morphological types of cell appendages on a strongly adhesive bacterium, *Acinetobacter* sp. strain Tol 5, Appl. Environ. Microbiol., 70 (2004) 5026–5029.
[23] L. Hall-Stoodley, P. Stoodley, Developmental regulation of microbial biofilms, Curr. Opin. Biotechnol., 13 (2002) 228–233.
[24] M. Herzberg, S. Kang, M. Elimelech, Role of extracellular polymeric substances (EPS) in biofouling of reverse osmosis membranes, Environ. Sci. Technol., 43 (2009) 4393–4398.
[25] C. Leroy, C. Delbarre, F. Ghillebaert, C. Compere, D. Combes, Influence of subtilisin on the adhesion of a marine bacterium which produces mainly proteins as extracellular polymers, J. Appl. Microbiol., 105 (2008) 791–799.
[26] J. Wingender, T.R. Neu, H.-C. Flemming, Microbial Extracellular Polymeric Substances: Characterization, Structure and Function, J. Wingender, T.R. Neu, H.-C. Flemming, Eds., Springer Berlin Heidelberg, Berlin, Heidelberg, 1999, pp. 1–19.
[27] R.D. Prescott, A.W. Decho, Flexibility and adaptability of quorum sensing in nature, Trends Microbiol., 28 (2020) 436–444.
[28] M.F. Siddiqui, M. Rzechowicz, W. Harvey, A.W. Zularisam, G.F. Anthony, Quorum sensing based membrane biofouling control for water treatment: a review, J. Water Process Eng., 7 (2015) 112–122.
[29] P. Chen, L. Cui, K. Zhang, Surface-enhanced Raman spectroscopy monitoring the development of dual-species biofouling on membrane surfaces, J. Membr. Sci., 473 (2015) 36–44.
[30] M. Klausen, A. Heydorn, P. Ragas, L. Lambertsen, A. Aaes-Jørgensen, S. Molin, T. Tolker-Nielsen, Biofilm formation by *Pseudomonas aeruginosa* wild type, flagella and type IV pili mutants, Mol. Microbiol., 48 (2003) 1511–1524.
[31] T. Joo-Hwa, L. Yu, Metabolic response of biofilm to shear stress in fixed-film culture, J. Appl. Microbiol., 90 (2001) 337–342.
[32] E. Poorasgari, T.V. Bugge, M.L. Christensen, M.K. Jørgensen, Compressibility of fouling layers in membrane bioreactors, J. Membr. Sci., 475 (2015) 65–70.
[33] S.S. Bucs, A.I. Radu, V. Lavric, J.S. Vrouwenvelder, C. Picioreanu, Effect of different commercial feed spacers on biofouling of reverse osmosis membrane systems: a numerical study, Desalination, 343 (2014) 26–37.
[34] R. Valladares Linares, S.S. Bucs, Z. Li, M. AbuGhdeeb, G. Amy, J.S. Vrouwenvelder, Impact of spacer thickness on biofouling in forward osmosis, Water Res., 57 (2014) 223–233.
[35] J. Chen, M. Zhang, A. Wang, H. Lin, H. Hong, X. Lu, Osmotic pressure effect on membrane fouling in a submerged anaerobic membrane bioreactor and its experimental verification, Bioresour. Technol., 125 (2012) 97–101.
[36] M. Herzberg, M. Elimelech, Biofouling of reverse osmosis membranes: role of biofilm-enhanced osmotic pressure, J. Membr. Sci., 295 (2007) 11–20.
[37] J. Su, S. Zhang, M.M. Ling, T.S. Chung, Forward osmosis: an emerging technology for sustainable supply of clean water, Clean Technol. Environ. Policy, 14 (2012) 507–511.
[38] K.W. Lawson, D.R. Lloyd, Membrane distillation, J. Membr. Sci., 124 (1997) 1–25.
[39] S.E. Kwan, E. Bar-Zeev, M. Elimelech, Biofouling in forward osmosis and reverse osmosis: measurements and mechanisms, J. Membr. Sci., 493 (2015) 703–708.
[40] W.A. Phillip, J.S. Yong, M. Elimelech, Reverse draw solute permeation in forward osmosis: modeling and experiments, Environ. Sci. Technol., 44 (2010) 5170–5176.
[41] M. Gryta, The assessment of microorganism growth in the membrane distillation system, Desalination, 142 (2002) 79–88.
[42] A. Bogler, E. Bar-Zeev, Membrane distillation biofouling: impact of feedwater temperature on biofilm characteristics and membrane performance, Environ. Sci. Technol., 52 (2018) 10019–10029.
[43] Y. Miura, Y. Watanabe, S. Okabe, Membrane biofouling in pilot-scale membrane bioreactors (MBRs) treating municipal wastewater: impact of biofilm formation, Environ. Sci. Technol., 41 (2007) 632–638.
[44] R. Xu, W. Qin, B. Zhang, X. Wang, T. Li, Y. Zhang, X. Wen, Nanofiltration in pilot scale for wastewater reclamation: long-term performance and membrane biofouling characteristics, Chem. Eng. J., 395 (2020) 125087, doi: 10.1016/j.cej.2020.125087.
[45] J.S. Vrouwenvelder, D. van der Kooij, Diagnosis, prediction and prevention of biofouling of NF and RO membranes, Desalination, 139 (2001) 65–71.
[46] H.F. Ridgway, H.C. Flemming, Microbial Adhesion and Biofouling of Reverse Osmosis Membranes, Reverse Osmosis Technol., Marcel Dekker, New York, 1988, pp. 429–481.
[47] A.H. Rose, History and scientific basis of microbial biodeterioration of materials, Econ. Microbiol., 6 (1981) 1–18.
[48] T. Wilson, Optical sectioning in confocal fluorescent microscopes, J. Microsc., 154 (1989) 143–156.
[49] P. Stiefel, S. Schmidt-Emrich, K. Maniura-Weber, Q. Ren, Critical aspects of using bacterial cell viability assays with the fluorophores SYTO9 and propidium iodide, BMC Microbiol., 15 (2015) 36, doi: 10.1186/s12866-015-0376-x.
[50] V.E. Centonze, J.G. White, Multiphoton excitation provides optical sections from deeper within scattering specimens than confocal imaging, Biophys. J., 75 (1998) 2015–2024.
[51] A. Schönle, S.W. Hell, Heating by absorption in the focus of an objective lens, Opt. Lett., 23 (1998) 325–327.
[52] J.M. Squirrell, D.L. Wokosin, J.G. White, B.D. Bavister, Long-term two-photon fluorescence imaging of mammalian embryos without compromising viability, Nat. Biotechnol., 17 (1999) 763–767.
[53] D.J. Hughes, U.K. Tirlapur, R. Field, Z. Cui, *In situ* 3D characterization of membrane fouling by yeast suspensions using two-photon femtosecond near infrared non-linear optical imaging, J. Membr. Sci., 280 (2006) 124–133.
[54] E.C. Jensen, Types of imaging, Part 2: an overview of fluorescence microscopy, Anat. Rec. Adv. Integr. Anat. Evol. Biol., 295 (2012) 1621–1627.
[55] H. Li, A.G. Fane, H.G.L. Coster, S. Vigneswaran, Direct observation of particle deposition on the membrane surface during crossflow microfiltration, J. Membr. Sci., 149 (1998) 83–97.
[56] M. Wagner, H. Horn, Optical coherence tomography in biofilm research: a comprehensive review, Biotechnol. Bioeng., 114 (2017) 1386–1402.
[57] F.J. Doucet, L. Maguire, J.R. Lead, Size fractionation of aquatic colloids and particles by cross-flow filtration: analysis by scanning electron and atomic force microscopy, Anal. Chim. Acta, 522 (2004) 59–71.
[58] F. Saffarimiandoab, B. Yavuzturk Gul, S. Erkoc-Ilter, S. Guclu, S. Unal, B. Tunaboylu, Y.Z. Menceloglu, I. Koyuncu, Evaluation of biofouling behavior of zwitterionic silane coated reverse osmosis membranes fouled by marine bacteria, Prog. Org. Coat., 134 (2019) 303–311.
[59] S.E. Kirk, J.N. Skepper, A.M. Donald, Application of environmental scanning electron microscopy to determine biological surface structure, J. Microsc., 233 (2009) 205–224.
[60] T. Lauvvik, R. Bakke, Biofilm thickness measurements by variance analysis of optical images, J. Microbiol. Methods, 20 (1994) 219–224.
[61] Y. Oshikane, T. Kataoka, M. Okuda, S. Hara, H. Inoue, M. Nakano, Observation of nanostructure by scanning near-field optical microscope with small sphere probe, Sci. Technol. Adv. Mater., 8 (2007) 181–185.

[62] D. Vobornik, S. Vobornik, Scanning near-field optical microscopy, Bosn. J. Basic Med. Sci., 8 (2008) 63–71.
[63] A.N. Cranin, Handbook of Biomaterials Evaluation. Scientific, Technical and Clinical Testing of Implant Materials, A.F. von Recum, Ed., MacMillan, New York, 1986. With a forward by Solomon Pollack and contributions by 61 authors and 10 section editors, Index, J. Biomed. Mater. Res., 21 (1987) 1167–1168.
[64] S. Chatterjee, N. Biswas, A. Datta, R. Dey, P. Maiti, Atomic force microscopy in biofilm study, Microscopy, 63 (2014) 269–278.
[65] Y.F. Dufrêne, T. Ando, R. Garcia, D. Alsteens, D. Martinez-Martin, A. Engel, C. Gerber, D.J. Müller, Imaging modes of atomic force microscopy for application in molecular and cell biology, Nat. Nanotechnol., 12 (2017) 295–307.
[66] J. Reichman, Handbook of Optical Filters for Fluorescence Microscopy, Chroma Technology Corp., Bellows Falls, VT, USA, 2013.
[67] A. García, B. Rodríguez, D. Oztürk, M. Rosales, C. Paredes, F. Cuadra, S. Montserrat, Desalination performance of antibiofouling reverse osmosis membranes, Mod Environ. Sci. Eng., 2 (2016) 481–489.
[68] L.A. Bereschenko, A.J.M. Stams, G.J.W. Euverink, M.C.M. van Loosdrecht, Biofilm formation on reverse osmosis membranes is initiated and dominated by *Sphingomonas* spp., Appl. Environ. Microbiol., 76 (2010) 2623–2632.
[69] M.M.T. Khan, P.S. Stewart, D.J. Moll, W.E. Mickols, M.D. Burr, S.E. Nelson, A.K. Camper, Assessing biofouling on polyamide reverse osmosis (RO) membrane surfaces in a laboratory system, J. Membr. Sci., 349 (2010) 429–437.
[70] M.M.T. Khan, P.S. Stewart, D.J. Moll, W.E. Mickols, S.E. Nelson, A.K. Camper, Characterization and effect of biofouling on polyamide reverse osmosis and nanofiltration membrane surfaces, Biofouling, 27 (2011) 173–183.
[71] M. Roldán, E. Clavero, M. Hernández-Mariné, Confocal Laser Scanning Microscopy of Aerophytic Biofilms, in: Cultural Heritage Research: A Pan-European Challenge, Proceedings of the 5th EC Conference, Cracow, Poland, 2002, pp. 320–323.
[72] A. Tárnok, SYTO dyes and histoproteins—myriad of applications, Cytometry, Part A, 73A (2008) 477–479.
[73] D. Prieto, G. Aparicio, M. Machado, F.R. Zolessi, Application of the DNA-specific stain methyl green in the fluorescent labeling of embryos, J. Vis. Exp., 99 (2015) e52769, doi:10.3791/52769.
[74] J.A. Kiernan, Localization of α-D-glucosyl and α-D-mannosyl groups of mucosubstances with concanavalin A and horseradish peroxidase, Histochemistry, 44 (1975) 39–45.
[75] T.H. Steinberg, R.P. Haugland, V.L. Singer, Applications of SYPRO orange and SYPRO red protein gel stains, Anal. Biochem., 239 (1996) 238–245.
[76] B. Yuan, X. Wang, C. Tang, X. Li, G. Yu, In situ observation of the growth of biofouling layer in osmotic membrane bioreactors by multiple fluorescence labeling and confocal laser scanning microscopy, Water Res., 75 (2015) 188–200.
[77] J. Luo, J. Zhang, X. Tan, D. McDougald, G. Zhuang, A.G. Fane, S. Kjelleberg, Y. Cohen, S.A. Rice, The correlation between biofilm biopolymer composition and membrane fouling in submerged membrane bioreactors, Biofouling, 30 (2014) 1093–1110.
[78] D. van der Kooij, W. Hijnen, C. Cristina, A. Brouwer-Hanzens, E. Cornelissen, Assessment of the Biofilm Removal Efficiency of Cleaning Agents and Procedures for RO/NF Membranes, Watercycle Research Institute, BTO Report - BTO 2011.056, Nieuwegein, 2012, pp. 1–86.
[79] D.S. Janjaroen, Role of Disinfectants and Pipe Materials on Bacterial Adhesion Onto Biofilms, University of Illinois at Urbana-Champaign, Urbana, Illinois, 2013.
[80] E. Drioli, A. Criscuoli, F. Macedonio, Membrane-Based Desalination: An Integrated Approach (MEDINA), IWA Publishing, 10 (2011), doi: 10.2166/9781780400914.
[81] A. Periasamy, P. Skoglund, C. Noakes, R. Keller, An evaluation of two-photon excitation versus confocal and digital deconvolution fluorescence microscopy imaging in *Xenopus morphogenesis*, Microsc. Res. Tech., 47 (1999) 172–181.
[82] D.J. Hughes, Z. Cui, R.W. Field, U.K. Tirlapur, Membrane fouling by cell-protein mixtures: in situ characterisation using multi-photon microscopy, Biotechnol. Bioeng., 96 (2007) 1083–1091.
[83] D.J. Hughes, Z. Cui, R.W. Field, U.K. Tirlapur, In situ three-dimensional characterization of membrane fouling by protein suspensions using multiphoton microscopy, Langmuir, 22 (2006) 6266–6272.
[84] R. Field, D. Hughes, Z. Cui, U. Tirlapur, Some observations on the chemical cleaning of fouled membranes, Desalination, 227 (2008) 132–138.
[85] Y. Marselina, P. Le-Clech, R. Stuetz, V. Chen, Detailed characterisation of fouling deposition and removal on a hollow fibre membrane by direct observation technique, Desalination, 231 (2008) 3–11.
[86] S.-T. Kang, A. Subramani, E.M.V. Hoek, M.A. Deshusses, M.R. Matsumoto, Direct observation of biofouling in cross-flow microfiltration: mechanisms of deposition and release, J. Membr. Sci., 244 (2004) 151–165.
[87] A. Subramani, E.M.V. Hoek, Direct observation of initial microbial deposition onto reverse osmosis and nanofiltration membranes, J. Membr. Sci., 319 (2008) 111–125.
[88] J. Wang, A.G. Fane, J.W. Chew, Understanding the anaerobic fluidized membrane bioreactor for wastewater treatment, European Water, 58 (2017) 371–374.
[89] P. Le-Clech, Y. Marselina, Y. Ye, R.M. Stuetz, V. Chen, Visualisation of polysaccharide fouling on microporous membrane using different characterisation techniques, J. Membr. Sci., 290 (2007) 36–45.
[90] Y. Marselina, Lifia, P. Le-Clech, R.M. Stuetz, V. Chen, Characterisation of membrane fouling deposition and removal by direct observation technique, J. Membr. Sci., 341 (2009) 163–171.
[91] Y. Ye, P. Le-Clech, Evolution of fouling deposition and removal on hollow fibre membrane during filtration with periodical backwash, Desalination, 283 (2011) 198–205.
[92] S. Lorenzen, Y. Ye, V. Chen, M.L. Christensen, Direct observation of fouling phenomena during cross-flow filtration: influence of particle surface charge, J. Membr. Sci., 510 (2016) 546–558.
[93] D. Huang, E.A. Swanson, C.P. Lin, J.S. Schuman, W.G. Stinson, W. Chang, M.R. Hee, T. Flotte, K. Gregory, C.A. Puliafito, J.G. Fujimoto, Optical coherence tomography, Science, 254 (1991) 1178–1181.
[94] I.D. Kilic, R. Serdoz, E. Fabris, F.A. Jaffer, C. Di Mario, Optical Coherence Tomography, Near-Infrared Spectroscopy, and Near-Infrared Fluorescence Molecular Imaging: Principles and Practice, in: Interventional Cardiology, John Wiley & Sons, Ltd., Chichester, UK, 2016, pp. 91–106.
[95] N.M. Israelsen, C.R. Petersen, A. Barh, D. Jain, M. Jensen, G. Hannesschläger, P. Tidemand-Lichtenberg, C. Pedersen, A. Podoleanu, O. Bang, Real-time high-resolution mid-infrared optical coherence tomography, Light Sci. Appl., 8 (2019) 11, doi: 10.1038/s41377-019-0122-5.
[96] J.G. Fujimoto, C. Pitris, S.A. Boppart, M.E. Brezinski, Optical coherence tomography: an emerging technology for biomedical imaging and optical biopsy, Neoplasia, 2 (2000) 9–25.
[97] W. Li, X. Liu, Y.-N. Wang, T.H. Chong, C.Y. Tang, A.G. Fane, Analyzing the evolution of membrane fouling via a novel method based on 3D optical coherence tomography imaging, Environ. Sci. Technol., 50 (2016) 6930–6939.
[98] L. Fortunato, Y. Jang, J.-G. Lee, S. Jeong, S. Lee, T. Leiknes, N. Ghaffour, Fouling development in direct contact membrane distillation: non-invasive monitoring and destructive analysis, Water Res., 132 (2018) 34–41.
[99] A. Bauer, M. Wagner, F. Saravia, S. Bartl, V. Hilgenfeldt, H. Horn, In-situ monitoring and quantification of fouling development in membrane distillation by means of optical coherence tomography, J. Membr. Sci., 577 (2019) 145–152.
[100] C. Haisch, R. Niessner, Visualisation of transient processes in biofilms by optical coherence tomography, Water Res., 41 (2007) 2467–2472.
[101] M. Wagner, D. Taherzadeh, C. Haisch, H. Horn, Investigation of the mesoscale structure and volumetric features of

biofilms using optical coherence tomography, Biotechnol. Bioeng., 107 (2010) 844–853.
[102] D. Janjaroen, F. Ling, G. Monroy, N. Derlon, E. Mogenroth, S.A. Boppart, W.-T. Liu, T.H. Nguyen, Roles of ionic strength and biofilm roughness on adhesion kinetics of *Escherichia coli* onto groundwater biofilm grown on PVC surfaces, Water Res., 47 (2013) 2531–2542.
[103] N. Derlon, N. Koch, B. Eugster, T. Posch, J. Pernthaler, W. Pronk, E. Morgenroth, Activity of metazoa governs biofilm structure formation and enhances permeate flux during gravity-driven membrane (GDM) filtration, Water Res., 47 (2013) 2085–2095.
[104] N. Derlon, M. Peter-Varbanets, A. Scheidegger, W. Pronk, E. Morgenroth, Predation influences the structure of biofilm developed on ultrafiltration membranes, Water Res., 46 (2012) 3323–3333.
[105] S. West, M. Wagner, C. Engelke, H. Horn, Optical coherence tomography for the in situ three-dimensional visualization and quantification of feed spacer channel fouling in reverse osmosis membrane modules, J. Membr. Sci., 498 (2016) 345–352.
[106] L. Fortunato, S. Bucs, R.V. Linares, C. Cali, J.S. Vrouwenvelder, T. Leiknes, Spatially-resolved in-situ quantification of biofouling using optical coherence tomography (OCT) and 3D image analysis in a spacer filled channel, J. Membr. Sci., 524 (2017) 673–681.
[107] L. Fortunato, T. Leiknes, In-situ biofouling assessment in spacer filled channels using optical coherence tomography (OCT): 3D biofilm thickness mapping, Bioresour. Technol., 229 (2017) 231–235.
[108] A. Inurria, P. Cay-Durgun, D. Rice, H. Zhang, D.-K. Seo, M.L. Lind, F. Perreault, Polyamide thin-film nanocomposite membranes with graphene oxide nanosheets: balancing membrane performance and fouling propensity, Desalination, 451 (2019) 139–147.
[109] C. Dreszer, A.D. Wexler, S. Drusová, T. Overdijk, A. Zwijnenburg, H.-C. Flemming, J.C. Kruithof, J.S. Vrouwenvelder, In-situ biofilm characterization in membrane systems using optical coherence tomography: formation, structure, detachment and impact of flux change, Water Res., 67 (2014) 243–254.
[110] L. Fortunato, S. Jeong, T. Leiknes, Time-resolved monitoring of biofouling development on a flat sheet membrane using optical coherence tomography, Sci. Rep., 7 (2017) 15, doi: 10.1038/s41598-017-00051-9.
[111] S. El Abed, F. Hamadi, H. Latrache, S.K. Ibnsouda, Scanning Electron Microscopy (SEM) and Environmental SEM: Suitable Tools for Study of Adhesion Stage and Biofilm Formation, INTECH Open Access Publisher, 2012.
[112] A. Storti, A.C. Pizzolitto, E.L. Pizzolitto, Detection of mixed microbial biofilms on central venous catheters removed from intensive care unit patients, Braz. J. Microbiol., 36 (2005) 275–280.
[113] G. Zhao, W.N. Chen, Biofouling formation and structure on original and modified PVDF membranes: role of microbial species and membrane properties, RSC Adv., 7 (2017) 37990–38000.
[114] W. Ma, M.S. Rahaman, H. Therien-Aubin, Controlling biofouling of reverse osmosis membranes through surface modification via grafting patterned polymer brushes, J. Water Reuse Desal., 5 (2015) 326–334.
[115] T.N. Tengku Sallehuddin, M. Abu Seman, Modification of thin-film composite nanofiltration membrane using silver nanoparticles: preparation, characterization and antibacterial performance, J. Membr. Sci. Res., 3 (2017) 29–35.
[116] H. Ivnitsky, I. Katz, D. Minz, G. Volvovic, E. Shimoni, E. Kesselman, R. Semiat, C.G. Dosoretz, Bacterial community composition and structure of biofilms developing on nanofiltration membranes applied to wastewater treatment, Water Res., 41 (2007) 3924–3935.
[117] M. Amouamouha, G.B. Gholikandi, M. Amouamouha, G. Badalians Gholikandi, Characterization and antibiofouling performance investigation of hydrophobic silver nanocomposite membranes: a comparative study, Membranes (Basel), 7 (2017) 64, doi: 10.3390/membranes7040064.
[118] C. Whittaker, H. Ridgway, B.H. Olson, Evaluation of cleaning strategies for removal of biofilms from reverse-osmosis membranes, Appl. Environ. Microbiol., 48 (1984) 395–403.
[119] S. Erkoc-Ilter, F. Saffarimiandoab, S. Guclu, D.Y. Koseoglu-Imer, B. Tunaboylu, Y. Menceloglu, I. Koyuncu, S. Unal, Surface modification of reverse osmosis desalination membranes with zwitterionic silane compounds for enhanced organic fouling resistance, Ind. Eng. Chem. Res., 60 (2021) 5133–5144.
[120] R. Chan, V. Chen, Characterization of protein fouling on membranes: opportunities and challenges, J. Membr. Sci., 242 (2004) 169–188.
[121] J.H. Priester, A.M. Horst, L.C. Van De Werfhorst, J.L. Saleta, L.A.K. Mertes, P.A. Holden, Enhanced visualization of microbial biofilms by staining and environmental scanning electron microscopy, J. Microbiol. Methods, 68 (2007) 577–587.
[122] M.G. Darkin, C. Gilpin, J.B. Williams, C.M. Sangha, Direct wet surface imaging of an anaerobic biofilm by environmental scanning electron microscopy: application to landfill clay liner barriers, Scanning, 23 (2006) 346–350.
[123] B. Little, P. Wagner, R. Ray, R. Pope, R. Scheetz, Biofilms: an ESEM evaluation of artifacts introduced during SEM preparation, J. Ind. Microbiol., 8 (1991) 213–221.
[124] E. Stabentheiner, A. Zankel, P. Pölt, Environmental scanning electron microscopy (ESEM)—a versatile tool in studying plants, Protoplasma, 246 (2010) 89–99.
[125] P. Le-Clech, Y. Marselina, R.M. Stuetz, V. Chen, Fouling Visualisation of Soluble Microbial Product Models in MBRs, Conference of the European Membrane Society (EUROMEMBRANE 2006), Giardini Naxos Italy, 24-28 September 2006, Elsevier, Amsterdam, Netherlands, 2006.
[126] Y.R. Teo, Y.K. Yong, A.J. Fleming, A Review of Scanning Methods and Control Implications for Scanning Probe Microscopy, 2016 American Control Conference (ACC), IEEE, Boston, MA, USA, 2016, pp. 7377–7383.
[127] C.V. Nguyen, C. So, R.M. Stevens, Y. Li, L. Delziet, P. Sarrazin, M. Meyyappan, High lateral resolution imaging with sharpened tip of multi-walled carbon nanotube scanning probe, J. Phys. Chem. B, 108 (2004) 2816–2821.
[128] M. Tomitori, T. Arai, Tip cleaning and sharpening processes for noncontact atomic force microscope in ultrahigh vacuum, Appl. Surf. Sci., 140 (1999) 432–438.
[129] G. Binnig, H. Rohrer, Ch. Gerber, E. Weibel, Surface studies by scanning tunneling microscopy, Phys. Rev. Lett., 49 (1982) 57, doi: 10.1103/PhysRevLett.49.57.
[130] S.-L. Guo, B.-L. Chen, S.A. Durrani, Chapter 3 – Solid-State Nuclear Track Detectors, M.F. L'Annunziata, Ed., Handbook of Radioactivity Analysis (Fourth Edition), Volume 1: Radiation Physics and Detectors, Academic Press, United States, 2012, pp. 233–298.
[131] E.-S. Kwak, T.J. Kang, D.A. Vanden Bout, Fluorescence lifetime imaging with near-field scanning optical microscopy, Anal. Chem., 73 (2001) 3257–3262.
[132] E. Betzig, A. Lewis, A. Harootunian, M. Isaacson, E. Kratschmer, Near field scanning optical microscopy (NSOM): development and biophysical applications, Biophys. J., 49 (1986) 269–279.
[133] R.C. Dunn, Near-field scanning optical microscopy, Chem. Rev., 99 (1999) 2891–2928.
[134] S. Vahabi, B. Nazemi Salman, A. Javanmard, Atomic force microscopy application in biological research: a review study, Iran. J. Med. Sci., 38 (2013) 76–83.
[135] Q. Zhong, D. Inniss, K. Kjoller, V.B. Elings, Fractured polymer/silica fiber surface studied by tapping mode atomic force microscopy, Surf. Sci., 290 (1993) L688–L692.
[136] H. Wang, P.K. Chu, Chapter 4 – Surface Characterization of Biomaterials, A. Bandyopadhyay, S. Bose, Eds., Characterization of Biomaterials, Elsevier, 2013, pp. 105–174.

[137] A.M. Zaky, I.C. Escobar, C.L. Gruden, Application of atomic force microscopy for characterizing membrane biofouling in the micrometer and nanometer scales, Environ. Prog. Sustainable Energy, 32 (2013) 449–457.
[138] S. Javdaneh, M.R. Mehrnia, M. Homayoonfal, Engineering design of a biofilm formed on a pH-sensitive ZnO/PSf nanocomposite membrane with antibacterial properties, RSC Adv., 6 (2016) 112269–112281.
[139] B. Tang, C. Yu, L. Bin, Y. Zhao, X. Feng, S. Huang, F. Fu, J. Ding, C. Chen, P. Li, Q. Chen, Essential factors of an integrated moving bed biofilm reactor–membrane bioreactor: adhesion characteristics and microbial community of the biofilm, Bioresour. Technol., 211 (2016) 574–583.
[140] C.J. Wright, I. Armstrong, The application of atomic force microscopy force measurements to the characterisation of microbial surfaces, Surf. Interface Anal., 38 (2006) 1419–1428.
[141] W.R. Bowen, N. Hilal, R.W. Lovitt, P.M. Williams, Atomic force microscope studies of membranes: surface pore structures of diaflo ultrafiltration membranes, J. Colloid Interface Sci., 180 (1996) 350–359.
[142] W. Richard Bowen, N. Hilal, R.W. Lovitt, A.O. Sharif, P.M. Williams, Atomic force microscope studies of membranes: force measurement and imaging in electrolyte solutions, J. Membr. Sci., 126 (1997) 77–89.
[143] S. Marka, S. Anand, Feed substrates influence biofilm formation on reverse osmosis membranes and their cleaning efficiency, J. Dairy Sci., 101 (2018) 84–95.
[144] L.C. Powell, N. Hilal, C.J. Wright, Atomic force microscopy study of the biofouling and mechanical properties of virgin and industrially fouled reverse osmosis membranes, Desalination, 404 (2017) 313–321.
[145] M.R. Gryk, J. Vyas, M.W. Maciejewski, Biomolecular NMR data analysis, Prog. Nucl. Magn. Reson. Spectrosc., 56 (2010) 329–345.
[146] J.H. Lee, Y. Okuno, S. Cavagnero, Sensitivity enhancement in solution NMR: emerging ideas and new frontiers, J. Magn. Reson., 241 (2014) 18–31.
[147] R.G. Evens, Economic costs of nuclear magnetic resonance imaging, J. Comput. Assisted Tomogr., 8 (1984) 200–203.
[148] Y. Li, M.E. Lacey, J. V Sweedler, A.G. Webb, Spectral restoration from low signal-to-noise, distorted NMR signals: application to hyphenated capillary electrophoresis-NMR, J. Magn. Reson., 162 (2003) 133–140.
[149] D.A. Graf von der Schulenburg, J.S. Vrouwenvelder, S.A. Creber, M.C.M. van Loosdrecht, M.L. Johns, Nuclear magnetic resonance microscopy studies of membrane biofouling, J. Membr. Sci., 323 (2008) 37–44.
[150] J. Schmitt, H.-C. Flemming, FTIR-spectroscopy in microbial and material analysis, Int. Biodeterior. Biodegrad., 41 (1998) 1–11.
[151] F. Humbert, F. Quilès, In-situ Study of Early Stages of Biofilm Formation Under Different Environmental Stresses by ATR-FTIR Spectroscopy, A. Mendez-Vilas, Ed., Science Against Microbial Pathogens: Communicating Current Research and Technological Advances, Formatex, Spain, 2011.
[152] F. Faghihzadeh, N.M. Anaya, L.A. Schifman, V. Oyanedel-Craver, Fourier transform infrared spectroscopy to assess molecular-level changes in microorganisms exposed to nanoparticles, Nanotechnol. Environ. Eng., 1 (2016) 1, doi: 10.1007/s41204-016-0001-8.
[153] R.M. Donlan, J.A. Piede, C.D. Heyes, L. Sanii, R. Murga, P. Edmonds, I. El-Sayed, M.A. El-Sayed, Model system for growing and quantifying *Streptococcus pneumoniae* biofilms in situ and in real time, Appl. Environ. Microbiol., 70 (2004) 4980–4988.
[154] L. Benavente, C. Coetsier, A. Venault, Y. Chang, C. Causserand, P. Bacchin, P. Aimar, FTIR mapping as a simple and powerful approach to study membrane coating and fouling, J. Membr. Sci., 520 (2016) 477–489.
[155] M.G. Albrecht, J.A. Creighton, Anomalously intense Raman spectra of pyridine at a silver electrode, J. Am. Chem. Soc., 99 (1977) 5215–5217.
[156] L. Cui, M. Yao, B. Ren, K.-S. Zhang, Sensitive and versatile detection of the fouling process and fouling propensity of proteins on polyvinylidene fluoride membranes via surface-enhanced raman spectroscopy, Anal. Chem., 83 (2011) 1709–1716.
[157] M. Kögler, B. Zhang, L. Cui, Y. Shi, M. Yliperttula, T. Laaksonen, T. Viitala, K. Zhang, Real-time Raman based approach for identification of biofouling, Sens. Actuators, B, 230 (2016) 411–421.
[158] L. Cui, P. Chen, B. Zhang, D. Zhang, J. Li, F.L. Martin, K. Zhang, Interrogating chemical variation via layer-by-layer SERS during biofouling and cleaning of nanofiltration membranes with further investigations into cleaning efficiency, Water Res., 87 (2015) 282–291.
[159] K. Huttenlochner, C. Müller-Renno, C. Ziegler, R. Merz, B. Merz, M. Kopnarski, J. Chodorski, C. Schlegel, R. Ulber, Removing biofilms from stainless steel without changing surface properties relevant for bacterial attachment, Biointerphases, 12 (2017) 02C404, doi: 10.1116/1.4982196.
[160] V.M. Huang, S.-L. Wu, M.E. Orazem, N. Pébère, B. Tribollet, V. Vivier, Local electrochemical impedance spectroscopy: a review and some recent developments, Electrochim. Acta, 56 (2011) 8048–8057.
[161] M.J. Franklin, D.E. Nivens, J.B. Guckert, D.C. White, Technical note: effect of electrochemical impedance spectroscopy on microbial biofilm cell numbers, viability, and activity, Corrosion, 47 (1991) 519–522.
[162] J.S. Ho, J.H. Low, L.N. Sim, R.D. Webster, S.A. Rice, A.G. Fane, H.G.L. Coster, In-situ monitoring of biofouling on reverse osmosis membranes: detection and mechanistic study using electrical impedance spectroscopy, J. Membr. Sci., 518 (2016) 229–242.
[163] A. Bax, S. Subramanian, Sensitivity-enhanced two-dimensional heteronuclear shift correlation NMR spectroscopy, J. Magn. Reson., 67 (1986) 565–569.
[164] D.S. Wishart, C.G. Bigam, J. Yao, F. Abildgaard, H.J. Dyson, E. Oldfield, J.L. Markley, B.D. Sykes, 1H, 13C and 15N chemical shift referencing in biomolecular NMR, J. Biomol. NMR, 6 (1995) 135–140.
[165] J.A. Detre, Magnetic Resonance Imaging, Neurobiol. Dis., 2007, pp. 793–800.
[166] S.A. Creber, T.R.R. Pintelon, D.A.W. Graf von der Schulenburg, J.S. Vrouwenvelder, M.C.M. van Loosdrecht, M.L. Johns, Magnetic resonance imaging and 3D simulation studies of biofilm accumulation and cleaning on reverse osmosis membranes, Food Bioprod. Process., 88 (2010) 401–408.
[167] J.S. Vrouwenvelder, C. Picioreanu, J.C. Kruithof, M.C.M. van Loosdrecht, Biofouling in spiral wound membrane systems: three-dimensional CFD model based evaluation of experimental data, J. Membr. Sci., 346 (2010) 71–85.
[168] E.O. Fridjonsson, S.J. Vogt, J.S. Vrouwenvelder, M.L. Johns, Early non-destructive biofouling detection in spiral wound RO membranes using a mobile earth's field NMR, J. Membr. Sci., 489 (2015) 227–236.
[169] J.R. Heber, E.A. Orvil, Infrared spectroscopy as a means for identification of bacteria, Science, 116 (1952) 111–112.
[170] V. Shapaval, B. Walczak, S. Gognies, T. Møretrø, H.P. Suso, A. Wold Åsli, A. Belarbi, A. Kohler, FTIR spectroscopic characterization of differently cultivated food related yeasts, Analyst, 138 (2013) 4129, doi: 10.1039/c3an00304c.
[171] V. Shapaval, J. Schmitt, T. Møretrø, H.P. Suso, I. Skaar, A.W. Åsli, D. Lillehaug, A. Kohler, Characterization of food spoilage fungi by FTIR spectroscopy, J. Appl. Microbiol., 114 (2013) 788–796.
[172] M. Lin, M. Al-Holy, H. Al-Qadiri, D.-H. Kang, A.G. Cavinato, Y. Huang, B.A. Rasco, Discrimination of intact and injured *Listeria monocytogenes* by Fourier transform infrared spectroscopy and principal component analysis, J. Agric. Food Chem., 52 (2004) 5769–5772.
[173] H.M. Al-Qadiri, M. Lin, M.A. Al-Holy, A.G. Cavinato, B.A. Rasco, Detection of sublethal thermal injury in *Salmonella enterica* serotype typhimurium and *Listeria monocytogenes*

using Fourier transform infrared (FTIR) spectroscopy (4000 to 600 cm^{-1}), J. Food Sci., 73 (2008) M54–M61.
[174] K.A. Puzey, P.J. Gardner, V.K. Petrova, C.W. Donnelly, G.A. Petrucci, Automated species and strain identification of bacteria in complex matrices using FTIR spectroscopy, Proc. SPIE 6954, Chemical, Biological, Radiological, Nuclear, and Explosives (CBRNE) Sensing IX, 695412 (17 April 2008).
[175] H.C. van der Mei, D. Naumann, H.J. Busscher, Grouping of streptococcus mitis strains grown on different growth media by FTIR, Infrared Phys. Technol., 37 (1996) 561–564.
[176] M.C. Curk, F. Peledan, J.C. Hubert, Fourier transform infrared (FTIR) spectroscopy for identifying *Lactobacillus* species, FEMS Microbiol. Lett., 123 (1994) 241–248.
[177] K.J. Howe, K.P. Ishida, M.M. Clark, Use of ATR/FTIR spectrometry to study fouling of microfiltration membranes by natural waters, Desalination, 147 (2002) 251–255.
[178] G.J. Ellis, M.C. Martin, Opportunities and challenges for polymer science using synchrotron-based infrared spectroscopy, Eur. Polym. J., 81 (2016) 505–531.
[179] M. Xie, W. Luo, S.R. Gray, Synchrotron Fourier transform infrared mapping: A novel approach for membrane fouling characterization, Water Res., 111 (2017) 375–381.
[180] N.R. Maddela, Z. Zhou, Z. Yu, S. Zhao, F. Meng, Functional determinants of extracellular polymeric substances in membrane biofouling: experimental evidence from pure-cultured sludge bacteria, Appl. Environ. Microbiol., 84 (2018) e00756-18.
[181] M.M. Rahman, S. Al-Sulaimi, A.M. Farooque, Characterization of new and fouled SWRO membranes by ATR/FTIR spectroscopy, Appl. Water Sci., 8 (2018) 183, doi: 10.1007/s13201-018-0806-7.
[182] K.C. Khulbe, B. Kruczek, G. Chowdhury, S. Gagné, T. Matsuura, S.P. Verma, Characterization of membranes prepared from PPO by Raman scattering and atomic force microscopy, J. Membr. Sci., 111 (1996) 57–70.
[183] R. Lamsal, S.G. Harroun, C.L. Brosseau, G.A. Gagnon, Use of surface enhanced Raman spectroscopy for studying fouling on nanofiltration membrane, Sep. Purif. Technol., 96 (2012) 7–11.
[184] T. Virtanen, S.-P. Reinikainen, M. Kögler, M. Mänttäri, T. Viitala, M. Kallioinen, Real-time fouling monitoring with Raman spectroscopy, J. Membr. Sci., 525 (2017) 312–319.
[185] L. Cui, S. Chen, K. Zhang, Effect of toxicity of Ag nanoparticles on SERS spectral variance of bacteria, Spectrochim. Acta, Part A, 137 (2015) 1061–1066.
[186] B.-Y. Chang, S.-M. Park, Electrochemical impedance spectroscopy, Annu. Rev. Anal. Chem., 3 (2010) 207–229.
[187] R. Sengur-Tasdemir, Z. Guler-Gokce, A. Sezai Sarac, I. Koyuncu, Determination of membrane protein fouling by UV spectroscopy and electrochemical impedance spectroscopy, Polym. Plast. Technol. Eng., 57 (2018) 59–69.
[188] H.G.L. Coster, T.C. Chilcott, A.C.F. Coster, Impedance spectroscopy of interfaces, membranes and ultrastructures, Bioelectrochem. Bioenerg., 40 (1996) 79–98.
[189] F. Gao, J. Wang, H. Zhang, H. Jia, Z. Cui, G. Yang, Role of ionic strength on protein fouling during ultrafiltration by synchronized UV-vis spectroscopy and electrochemical impedance spectroscopy, J. Membr. Sci., 563 (2018) 592–601.
[190] J.M. Kavanagh, S. Hussain, T.C. Chilcott, H.G.L. Coster, Fouling of reverse osmosis membranes using electrical impedance spectroscopy: measurements and simulations, Desalination, 236 (2009) 187–193.
[191] L.N. Sim, Z.J. Wang, J. Gu, H.G.L. Coster, A.G. Fane, Detection of reverse osmosis membrane fouling with silica, bovine serum albumin and their mixture using in-situ electrical impedance spectroscopy, J. Membr. Sci., 443 (2013) 45–53.
[192] J.S. Park, J.H. Choi, K.H. Yeon, S.H. Moon, An approach to fouling characterization of an ion-exchange membrane using current-voltage relation and electrical impedance spectroscopy, J. Colloid Interface Sci., 294 (2006) 129–138.
[193] J.S. Park, T.C. Chilcott, H.G.L. Coster, S.H. Moon, Characterization of BSA-fouling of ion-exchange membrane systems using a subtraction technique for lumped data, J. Membr. Sci., 246 (2005) 137–144.
[194] J. Cen, M. Vukas, G. Barton, J. Kavanagh, H.G.L. Coster, Real time fouling monitoring with electrical impedance spectroscopy, J. Membr. Sci., 484 (2015) 133–139.
[195] J.S. Ho, L.N. Sim, R.D. Webster, B. Viswanath, H.G.L. Coster, A.G. Fane, Monitoring fouling behavior of reverse osmosis membranes using electrical impedance spectroscopy: a field trial study, Desalination, 407 (2017) 75–84.
[196] E.A. Genceli, R. Sengur-Tasdemir, G.M. Urper, S. Gumrukcu, Z. Guler-Gokce, U. Dagli, T. Turken, A.S. Sarac, I. Koyuncu, Effects of carboxylated multi-walled carbon nanotubes having different outer diameters on hollow fiber ultrafiltration membrane fabrication and characterization by electrochemical impedance spectroscopy, Polym. Bull., 75 (2018) 2431–2457.
[197] H. Ivnitsky, I. Katz, D. Minz, E. Shimoni, Y. Chen, J. Tarchitzky, R. Semiat, C.G. Dosoretz, Characterization of membrane biofouling in nanofiltration processes of wastewater treatment, Desalination, 185 (2005) 255–268.
[198] C.M. Pang, W.-T. Liu, community structure analysis of reverse osmosis membrane biofilms and the significance of *Rhizobiales* bacteria in biofouling, Environ. Sci. Technol., 41 (2007) 4728–4734.
[199] W. Zhi, Z. Ge, Z. He, H. Zhang, Methods for understanding microbial community structures and functions in microbial fuel cells: a review, Bioresour. Technol., 171 (2014) 461–468.
[200] H.W. Kim, H.S. Oh, S.R. Kim, K.B. Lee, K.M. Yeon, C.H. Lee, S. Kim, J.K. Lee, Microbial population dynamics and proteomics in membrane bioreactors with enzymatic quorum quenching, Appl. Microbiol. Biotechnol., 97 (2013) 4665–4675.
[201] B. Yavuzturk Gul, D.Y. Imer, P.-K. Park, I. Koyuncu, Evaluation of a novel anti-biofouling microorganism (*Bacillus* sp. T5) for control of membrane biofouling and its effect on bacterial community structure in membrane bioreactors., Water Sci. Technol., 77 (2018) 971–978.
[202] B.Y. Gül, D.Y. Imer, P.-K. Park, I. Koyuncu, Selection of quorum quenching (QQ) bacteria for membrane biofouling control: effect of different gram-staining QQ bacteria, *Bacillus* sp. T5 and *Delftia* sp. T6, on microbial population in membrane bioreactors, Water Sci. Technol., 78 (2018) 358–366.
[203] Y.L. Huang, J.S. Ki, R.J. Case, P.Y. Qian, Diversity and acyl-homoserine lactone production among subtidal biofilm-forming bacteria, Aquat. Microb. Ecol., 52 (2008) 185–193.
[204] R.I. Amann, W. Ludwig, K.H. Schleifer, Phylogenetic identification and in situ detection of individual microbial cells without cultivation, Microbiol. Rev., 59 (1995) 143–169.
[205] A. Poli, B. Nicolaus, A.A. Denizci, B. Yavuzturk, D. Kazan, *Halomonas smyrnensis* sp. nov., a moderately halophilic, exopolysaccharide-producing bacterium, Int. J. Syst. Evol. Microbiol., 63 (2013) 10–18.
[206] S. Lim, S. Kim, K.M. Yeon, B.I. Sang, J. Chun, C.H. Lee, Correlation between microbial community structure and biofouling in a laboratory scale membrane bioreactor with synthetic wastewater, Desalination, 287 (2012) 209–215.
[207] C.L. Chen, W.T. Liu, M.L. Chong, M.T. Wong, S.L. Ong, H. Seah, W.J. Ng, Community structure of microbial biofilms associated with membrane-based water purification processes as revealed using a polyphasic approach, Appl. Microbiol. Biotechnol., 63 (2004) 466–473.
[208] L.A. Bereschenko, G.H.J. Heilig, M.M. Nederlof, M.C.M. Van Loosdrecht, A.J.M. Stams, G.J.W. Euverink, Molecular characterization of the bacterial communities in the different compartments of a full-scale reverse-osmosis water purification plant, Appl. Environ. Microbiol., 74 (2008) 5297–5304.
[209] A.S. Ziegler, S.J. McIlroy, P. Larsen, M. Albertsen, A.A. Hansen, N. Heinen, P.H. Nielsen, Dynamics of the fouling layer microbial community in a membrane bioreactor, PLoS One, 11 (2016) e0158811, doi: 10.1371/journal.pone.0158811.

[210] S. Mikhaylin, L. Bazinet, Fouling on ion-exchange membranes: classification, characterization and strategies of prevention and control, Adv. Colloid Interface Sci., 229 (2015) 34–56.
[211] S. Jeong, K. Cho, H. Bae, P. Keshvardoust, S.A. Rice, S. Vigneswaran, S. Lee, T. Leiknes, Effect of microbial community structure on organic removal and biofouling in membrane adsorption bioreactor used in seawater pretreatment, Chem. Eng. J., 294 (2016) 30–39.
[212] A. Al Ashhab, O. Gillor, M. Herzberg, Biofouling of reverse-osmosis membranes under different shear rates during tertiary wastewater desalination: microbial community composition., Water Res., 67 (2014) 86–95.
[213] C.M. Pang, W.-T. Liu, Community structure analysis of reverse osmosis membrane biofilms and the significance of Rhizobiales bacteria in biofouling, Environ. Sci. Technol., 41 (2007) 4728–4734.
[214] R. Amann, B.M. Fuchs, S. Behrens, The identification of microorganisms by fluorescence in situ hybridisation, Curr. Opin. Biotechnol., 12 (2001) 231–236.
[215] G. Muyzer, E.C. de Waal, A.G. Uitterlinden, Profiling of complex microbial populations by denaturing gradient gel electrophoresis analysis of polymerase chain reaction-amplified genes coding for 16S rRNA, Appl. Environ. Microbiol., 59 (1993) 695–700.
[216] A. Drews, Membrane fouling in membrane bioreactors – characterisation, contradictions, cause and cures, J. Membr. Sci., 363 (2010) 1–28.
[217] H. Luo, P. Xu, Z. Ren, Long-term performance and characterization of microbial desalination cells in treating domestic wastewater, Bioresour. Technol., 120 (2012) 187–193.
[218] A. Piasecka, R. Bernstein, F. Ollevier, F. Meersman, C. Souffreau, R.M. Bilad, K. Cottenie, L. Vanysacker, C. Denis, I. Vankelecom, Study of biofilms on PVDF membranes after chemical cleaning by sodium hypochlorite, Sep. Purif. Technol., 141 (2015) 314–321.
[219] J. Cho, G. Amy, J. Pellegrino, Y. Yoon, Characterization of clean and natural organic matter (NOM) fouled NF and UF membranes, and foulants characterization, Desalination, 118 (1998) 101–108.
[220] F. Zhao, K. Xu, H. Ren, L. Ding, J. Geng, Y. Zhang, Combined effects of organic matter and calcium on biofouling of nanofiltration membranes, J. Membr. Sci., 486 (2015) 177–188.
[221] R. Glud, N. Ramsing, J. Gundersen, I. Klimant, Planar optrodes:a new tool for fine scale measurements of two-dimensional O_2 distribution in benthic communities, Mar. Ecol. Prog. Ser., 140 (1996) 217–226.
[222] E.I. Prest, M. Staal, M. Kühl, M.C.M. van Loosdrecht, J.S. Vrouwenvelder, Quantitative measurement and visualization of biofilm O_2 consumption rates in membrane filtration systems, J. Membr. Sci., 392–393 (2012) 66–75.
[223] N.M. Farhat, M. Staal, A. Siddiqui, S.M. Borisov, S.S. Bucs, J.S. Vrouwenvelder, Early non-destructive biofouling detection and spatial distribution: application of oxygen sensing optodes, Water Res., 83 (2015) 10–20.
[224] M. Staal, E.I. Prest, J.S. Vrouwenvelder, L.F. Rickelt, M. Kühl, A simple optode based method for imaging O_2 distribution and dynamics in tap water biofilms, Water Res., 45 (2011) 5027–5037.
[225] N.M. Farhat, J.S. Vrouwenvelder, M.C.M. Van Loosdrecht, S.S. Bucs, M. Staal, Effect of water temperature on biofouling development in reverse osmosis membrane systems, Water Res., 103 (2016) 149–159.
[226] N.M. Farhat, M. Staal, S.S. Bucs, M.C.M. Van Loosdrecht, J.S. Vrouwenvelder, Spatial heterogeneity of biofouling under different cross-flow velocities in reverse osmosis membrane systems, J. Membr. Sci., 520 (2016) 964–971.
[227] P. van den Brink, F. Vergeldt, H. Van As, A. Zwijnenburg, H. Temmink, M.C.M. van Loosdrecht, Potential of mechanical cleaning of membranes from a membrane bioreactor, J. Membr. Sci., 429 (2013) 259–267.
[228] J. Kappelhof, H.S. Vrouwenvelder, M. Schaap, J.C. Kruithof, D. Van Der Kooij, J.C. Schippers, An in situ biofouling monitor for membrane systems, Water Sci. Technol. Water Supply, 3 (2003) 205–210.
[229] C. Causserand, P. Aimar, Characterization of Filtration Membranes, Comprehensive Membrane Science and Engineering, 2010, pp. 311–335.
[230] M. Nyström, A. Pihlajamäki, N. Ehsani, Characterization of ultrafiltration membranes by simultaneous streaming potential and flux measurements, J. Membr. Sci., 87 (1994) 245–256.
[231] M.-S. Chun, W.C. Park, Time evolution of electrokinetic flow-induced streaming potential and flux in dead-end and cross-flow filtration of colloids through nanopores, J. Membr. Sci., 243 (2004) 417–424.
[232] M.-S. Chun, H. Il Cho, I.K. Song, Electrokinetic behavior of membrane zeta potential during the filtration of colloidal suspensions, Desalination, 148 (2002) 363–368.
[233] I. Petrinić, T. Pušić, I. Mijatović, B. Simončič, S. Šostar Turk, Characterization of polymeric nanofiltration membranes, Kem. u Ind., 56 (2007) 561–567.
[234] B. Teychene, P. Loulergue, C. Guigui, C. Cabassud, Development and use of a novel method for in line characterisation of fouling layers electrokinetic properties and for fouling monitoring, J. Membr. Sci., 370 (2011) 45–57.
[235] H. Jia, H. Zhang, J. Wang, H. Zhang, X. Zhang, Response of zeta potential to different types of local membrane fouling in dead-end membrane filtration with yeast suspension, RSC Adv., 5 (2015) 78738–78744.